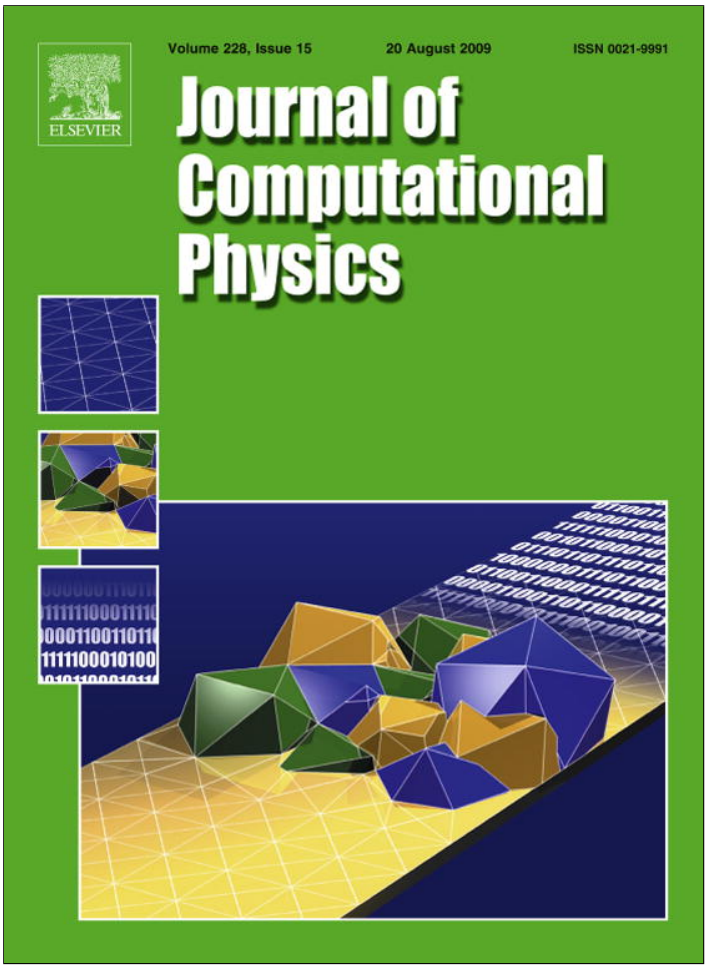

Journal of Computational Physics 228 (2009) 5390–5409

Contents lists available at ScienceDirect

Journal of Computational Physics

journal homepage: www.elsevier.com/locate/jcp

Reconstruction of spectral function from effective permittivity of a composite material using rational function approximations

Dali Zhang [a], Elena Cherkaev [b,*]

[a] Department of Mathematics and Statistics, University of Calgary, 2500 University Drive NW, Calgary, Alberta, Canada T2N 1N4
[b] Department of Mathematics, University of Utah, 155 South 1400 East, JWB 233, Salt Lake City, UT 84112, USA

ARTICLE INFO

Article history:
Received 12 April 2008
Received in revised form 13 April 2009
Accepted 15 April 2009
Available online 22 April 2009

Keywords:
Stieltjes representation
Padé approximation
Effective complex permittivity
Two-component composite

ABSTRACT

The paper deals with the problem of reconstruction of microstructural information from known effective complex permittivity of a composite material. A numerical method for recovering geometric information from measurements of frequency dependent effective complex permittivity is developed based on Stieltjes analytic representation of the effective permittivity tensor of a two-component mixture. We derive the Stieltjes representation for the effective permittivity of the medium using the eigenfunction expansion of the solution of a boundary-value problem. The spectral function in this representation contains all information about the microgeometry of the mixture. A discrete approximation of the spectral measure is derived from a rational (Padé) approximation followed by its partial fractions decomposition. The approach is based on the least squares minimization with regularization constraints provided by the spectral properties of the operator. The method is applied to calculation of volume fractions of the components in a mixture of two materials in a Bruggeman effective medium analytic model which has a continuous spectral density and to analytical models of two-phase composites with coated cylindrical and ellipsoidal inclusions. The numerical results of reconstruction of spectral measure for a mixture of silver and silicon dioxide and a composite of magnesium and magnesium fluoride show good agreement between theoretical and predicted values. The approach is applicable to geological materials, biocomposites, porous media, etc.

1. Introduction

The present paper deals with a problem of estimation of microstructural parameters in finely-structured heterogeneous mixtures from measured effective properties of the medium. There are numerous examples of such media: porous rock samples, mixtures of air bubbles and liquid, water droplets in clouds, biological tissues, and artificial composites. In these heterogeneous materials the scale of microstructure is much smaller than the wavelength of the applied electromagnetic signal, so that the measurements of the effective complex permittivity contain only "averaged" or "homogenized" information about the structure.

The problem of extraction of structural information from measured transport properties of composite materials was first introduced in [32] for estimating volume fractions of constituents in the composite. The approach is based on the analytic Stieltjes integral representation of the complex effective permittivity ϵ^* of a mixture of two materials with complex permittivity ϵ_1 and ϵ_2 developed in [3–5,24,34,35] in the course of constructing bounds for the effective complex permittivity ϵ^* of composite materials.

* Corresponding author. Tel.: +1 801 581 7315; fax: +1 801 581 4148.
E-mail addresses: dlzhang@math.ucalgary.ca (D. Zhang), elena@math.utah.edu (E. Cherkaev).

0021-9991/$ - see front matter © 2009 Elsevier Inc. All rights reserved.
doi:10.1016/j.jcp.2009.04.014

In [12], the problem of estimation of microstructural information from measured effective property was formulated as an inverse problem for the spectral measure in the Stieltjes analytic representation. Uniqueness of reconstruction of the spectral measure shown in [12] gives a basis for theory of inverse homogenization. Approaches to extraction of information about the geometry of the composite are mainly based on reconstruction of the spectral function [12–17,37,44,45] or on estimation of its first several moments [11,18,21,22,32,33,43]. It was shown that the problem of reconstruction of the spectral function is ill-posed and requires regularization [12]. Several regularized algorithms were developed in [12–14,45]. Rational approximation of the spectral function was introduced in [45]. The explicit formulas for inverse bounds on the volume fraction of one material in composite were derived in [43] for anisotropic composite materials (first order bounds) and in [11] for isotropic composites (second order bounds). Developed methods were applied to measurements of various properties of composites, such as multifrequency data for thin silver films [33], reflectivity measurements at different temperatures in [17]. Inverse bounds [43] were applied to estimation of volume fraction of a polarizable component from multifrequency measurements of the effective complex conductivity of a geophysical mixture. First and second order inverse bounds developed in [11] were used to estimate sea ice brine volume from actual measurements of the effective complex permittivity of sea ice. Extension to viscoelastic composites was developed in [9].

Here we consider a heterogeneous composite material which is formed of two homogeneous, isotropic phases with permittivity ϵ_1 and ϵ_2, and assume that the composite has a well-defined three dimensional periodic structure. We assume that the period of the microstructure of the mixture is small compared to the wavelength of applied electromagnetic fields. The complex permittivity function is oscillating on a fine scale. For an electric field $\mathbf{E}$ applied to the composite, the effective permittivity tensor ϵ^* is defined as a coefficient of proportionality between the averaged displacement $<\mathbf{D}>$ and averaged electric $<\mathbf{E}>$ fields: $<\mathbf{D}> = \epsilon^* <\mathbf{E}>$.

In order to derive the analytic representation of the effective permittivity tensor ϵ^* we start with formulation of a problem for the electric potential subject to appropriate Dirichlet and periodic boundary conditions. The weak solutions of the problem are used to derive a discrete approximation of the analytic Stieltjes representation based on the eigenfunction expansions of the solution of the Dirichlet periodic boundary-value problem. The information about the microgeometry of the mixture is contained in the spectral measure in this analytic representation

$$\mathbf{F}(s) = \mathbf{I}_3 - \frac{\epsilon^*}{\epsilon_2} = \int_0^1 \frac{\mathrm{d}\boldsymbol{\mu}(z)}{s - z}, \quad s = \frac{1}{1 - \epsilon_1/\epsilon_2}, \tag{1}$$

where $\mathbf{I}_3$ denotes the 3×3 identity matrix. Here the positive measure $\boldsymbol{\mu}$ is the spectral measure of a self-adjoint operator $\Gamma\chi$, with χ being the characteristic function of the domain occupied by the first material in the composite, and $\Gamma = \nabla(-\Delta)^{-1}(\nabla\cdot)$, where $(-\Delta)$ is the Laplacian operator. The tensor function $\mathbf{F}(s)$ is analytic outside the $[0,1]$-interval in the complex s-plane. The spectral representation (1) separates the dependence of the effective permittivity ϵ^* on the properties of the components from the dependence on the micro-geometry through the complex variable s. It was shown in [12] that the problem of reconstruction of the spectral measure $\boldsymbol{\mu}$ has unique solution if the values of ϵ^* are available on an arc in the complex s-plane. However, from the computation point of view, the problem of reconstruction of the spectral measure is extremely ill-posed. To obtain a stable reconstruction of the spectral measure, a new inversion method based on constrained rational approximation of the spectral function is developed in the present paper. The rational approximation of the spectral function is obtained from the solution of a constrained minimization problem followed by the partial fractions decomposition. To demonstrate the validity of the algorithm, the developed inversion method is applied to the reconstruction of spectral functions of composites in several analytic examples corresponding to composites with different structures. The chosen analytic models, have a continuous spectral density function as well as a combination of delta-functions. The results of numerical experiments for estimating volume fractions of the constituents for metal–insulator composite materials from the recovered spectral functions show good agreement between theoretical and predicted values.

The paper is organized as follows. Section 2 deals with an elliptic boundary-value problem for the electric potential with Dirichlet boundary conditions on a part of the boundary and periodic conditions on the rest of the boundary. In Section 3, we use the formulated solutions to the electric potential problem to derive a discrete approximation of the analytic Stieltjes representation for the effective permittivity tensor of an anisotropic two-phase composite material based on eigenfunction expansion of the solution. An inversion algorithm based on rational (Padé) approximation of the spectral function for given effective permittivity measurements is presented in Section 4. In Section 5, we derive spectral representations for analytical models of two-phase composite with cylindrical and ellipsoidal inclusions. We also used the three-dimensional Bruggeman self-consistent effective medium analytic model which has a continuous spectral density, to numerically demonstrate the efficiency of the method. Numerical experiments of reconstruction of the spectral function and estimation of the fractions of components in a mixture of silver and silicon dioxide and in a composite of magnesium and magnesium fluoride are shown in Section 6. The approach we present here, avoids specific assumptions about the microgeometry of the medium and works efficiently for any two-phase composite material. It can be used to evaluate material (structure) properties from measured effective complex permittivity or other properties of the composite.

2. Boundary value problem for the electric potential

We consider a heterogeneous composite medium occupying a cubic region $\Omega = \{\mathbf{y} = (y_1, y_2, y_3)^\top \mid 0 \leqslant y_i \leqslant L,\ i = 1,2,3\}$ in $\mathbb{R}^3$. The medium is a binary mixture of materials consisting of two homogeneous, isotropic phases with permittivity ϵ_1 in

the region Ω_1, and ϵ_2 in the region Ω_2, with $\Omega = \Omega_1 \cup \Omega_2$. Let χ be the characteristic function of the region Ω_1 occupied by the first component,

$$\chi(\mathbf{y}) = \begin{cases} 1, & \text{if } \mathbf{y} \in \Omega_1, \\ 0, & \text{otherwise}, \end{cases} \tag{2}$$

which is periodic on the boundary of Ω. The characteristic function of the domain occupied by the second component is $1 - \chi(\mathbf{y})$. The complex permittivity of the medium is defined as

$$\epsilon(\mathbf{y}) = \epsilon_1\chi(\mathbf{y}) + \epsilon_2(1 - \chi(\mathbf{y})), \quad \mathbf{y} \in \Omega. \tag{3}$$

It is supposed that the wavelength of applied electromagnetic field is much larger than the scale of inhomogeneities of the microstructure. If an electric field $\mathbf{E}$ is applied to the mixture, then in quasi-static approximation, low frequency Maxwell equations governing the fields in the composite are:

$$\nabla \cdot \mathbf{D} = 0, \quad \nabla \times \mathbf{E} = 0. \tag{4}$$

The constitutive relation between the displacement field $\mathbf{D}$ and electric field $\mathbf{E}$ is $\mathbf{D}(\mathbf{y}) = \epsilon(\mathbf{y})\mathbf{E}(\mathbf{y})$. Let the average electric field be $< \mathbf{E} > = \mathbf{e}_i$, and $\nabla\psi^{(i)}$ be a perturbation of the constant field $\mathbf{e}_i$, so that $\mathbf{E} = \nabla\psi^{(i)} + \mathbf{e}_i$. Here $\mathbf{e}_i$ is the unit vector in the ith direction ($i = 1,2,3$). Then the electric potential $\psi^{(i)}$ satisfies equation:

$$\nabla \cdot (\epsilon_1\chi(\mathbf{y}) + \epsilon_2(1 - \chi(\mathbf{y})))(\nabla\psi^{(i)} + \mathbf{e}_i) = 0, \quad \mathbf{y} \in \Omega \tag{5}$$

for a periodic medium.

Let $\mathbf{U} = (u^{(1)}, u^{(2)}, u^{(3)})^\top$ where $\nabla u^{(i)} = \nabla\psi^{(i)} + \mathbf{e}_i$ ($i = 1,2,3$) and the symbol $(\cdot)^\top$ indicates a transposed matrix. Then the effective permittivity tensor ϵ^* is defined as the coefficient of proportionality between the averaged fields

$$< \mathbf{D} >= \epsilon^* < \mathbf{E} > \tag{6}$$

and ϵ^* can be written as

$$\epsilon^* = \frac{1}{V}\int_\Omega \epsilon\nabla\mathbf{U}d\mathbf{y}, \quad \frac{1}{V}\int_\Omega \nabla\mathbf{U}d\mathbf{y} = \mathbf{I}_3, \tag{7}$$

where $\mathbf{I}_3$ is the 3×3 identity matrix and V is the volume of Ω.

The aim of this section is to construct a solution to the problem for the electric potential $u^{(i)}$ ($i = 1,2,3$)

$$\nabla \cdot \epsilon\nabla u^{(i)} = 0 \tag{8}$$

subject to the following non-homogeneous boundary conditions:

$$\begin{aligned} &u^{(i)} = \begin{cases} 0, & y_i = 0, \\ L, & y_i = L, \end{cases} \\ &u^{(i)}|_{\partial_{(j-)}\Omega} = u^{(i)}|_{\partial_{(j+)}\Omega}, \quad \left.\frac{\partial u^{(i)}}{\partial n}\right|_{\partial_{(j-)}\Omega} + \left.\frac{\partial u^{(i)}}{\partial n}\right|_{\partial_{(j+)}\Omega} = 0, \end{aligned} \tag{9}$$

where $\partial_{(j-)}\Omega \| \partial_{(j+)}\Omega$ ($i = 1,2,3$; $j \neq i$). Fig. 1 shows the geometry of a typical cell Ω with Dirichlet boundary conditions in y_3-direction and periodic boundary conditions in y_1-and y_2-directions for the electric potential $u^{(3)}$ in the composite with a periodic structure.

In order to obtain the solution of the Dirichlet and periodic boundary value problem (8) and (9), we first analyze the solvability of the homogeneous boundary value problem

$$\nabla \cdot \epsilon(\nabla\psi^{(i)} + \mathbf{e}_i) = 0, \quad i = 1,2,3, \tag{10}$$

$$\psi^{(i)}|_{y_i=0} = \psi^{(i)}|_{y_i=L} = 0,$$

$$\psi^{(i)}|_{\partial_{(j-)}\Omega} = \psi^{(i)}|_{\partial_{(j+)}\Omega}, \quad \left.\frac{\partial\psi^{(i)}}{\partial n}\right|_{\partial_{(j-)}\Omega} + \left.\frac{\partial\psi^{(i)}}{\partial n}\right|_{\partial_{(j+)}\Omega} = 0, \quad j \neq i, \tag{11}$$

where the part of the boundary $\partial_{(j-)}\Omega$ is parallel to $\partial_{(j+)}\Omega$. From (10) and (11), it can be seen that the electric potential function

$$u^{(i)} = y_i + \psi^{(i)} \quad (i = 1,2,3) \tag{12}$$

solves the boundary value problem (8) and (9).

Introducing the material parameter s,

$$s = \frac{\epsilon_2}{\epsilon_2 - \epsilon_1} \tag{13}$$

and representing the scalar complex permittivity $\epsilon(\mathbf{y})$ as

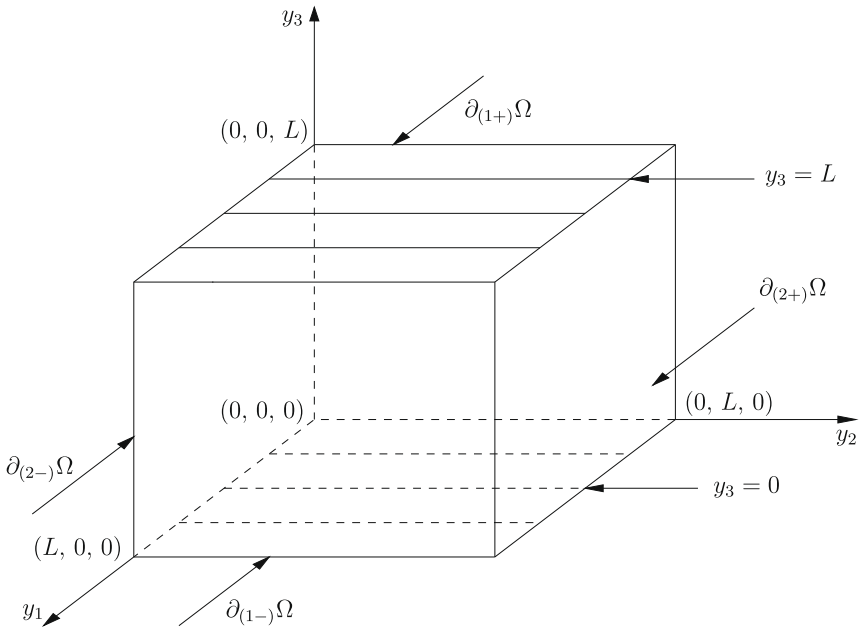

Fig. 1. Geometry of a periodic cell for the electric potential $u^{(3)}$.

$$\epsilon(\mathbf{y}) = \epsilon_1\chi(\mathbf{y}) + \epsilon_2(1-\chi(\mathbf{y})) = \epsilon_2\left(1 - \frac{1}{s}\chi(\mathbf{y})\right), \quad \mathbf{y} \in \Omega, \tag{14}$$

the boundary value problem (10) and (11) can be rewritten as

$$s\Delta\psi^{(i)} = \nabla\cdot\chi\left(\nabla\psi^{(i)} + \mathbf{e}_i\right) \tag{15}$$

with boundary conditions (11). We introduce the Green's function $G_i(\mathbf{y},\mathbf{y}')$ for the Laplace's problem [1]

$$\begin{aligned}
&\Delta G_i(\mathbf{y},\mathbf{y}') = -\delta(\mathbf{y}-\mathbf{y}') + \frac{1}{V},\\
&G_i|_{y_i=0} = G_i|_{y_i=L} = 0,\\
&G_i|_{\partial_{(j-)}\Omega} = G_i|_{\partial_{(j+)}\Omega}, \quad \left.\frac{\partial G_i}{\partial n}\right|_{\partial_{(j-)}\Omega} + \left.\frac{\partial G_i}{\partial n}\right|_{\partial_{(j+)}\Omega} = 0,
\end{aligned} \tag{16}$$

where $\delta(\mathbf{y})$ is the Dirac delta function and $\partial_{(j-)}\Omega \| \partial_{(j+)}\Omega$ ($i = 1,2,3$; $j \neq i$).

The problems (16) for different i, $i = 1,2,3$, differ only by coordinate rotations; since the Laplace operator is invariant to rotation of coordinates, the Green's functions $G_i(\mathbf{y},\mathbf{y}')$ for different i could be obtained by rotation. We use the Green's second identity for the function $\psi^{(i)}$:

$$\int_\Omega \left(\psi^{(i)}\Delta G_i - G_i\Delta\psi^{(i)}\right)d\mathbf{y} = \int_{\partial\Omega}\left(\psi^{(i)}\frac{\partial G_i}{\partial n} - G_i\frac{\partial\psi^{(i)}}{\partial n}\right)ds. \tag{17}$$

It can be seen that the boundary integral on the right hand side of (17) vanishes due to the boundary conditions for functions $\psi^{(i)}$ and $G_i(\mathbf{y},\mathbf{y}')$ on $\partial\Omega$. Using (15) and (16) in the left hand side of (17), we bring Eq. (17) to the form:

$$-\int_\Omega \psi^{(i)}\delta(\mathbf{y}-\mathbf{y}')d\mathbf{y}' + \frac{1}{V}\int_\Omega \psi^{(i)}d\mathbf{y}' = \frac{1}{s}\int_\Omega G_i(\mathbf{y},\mathbf{y}')\nabla\cdot\chi(\nabla\psi^{(i)} + \mathbf{e}_i)d\mathbf{y}'. \tag{18}$$

Thus, (18) implies that the solution of the boundary value problem (10) and (11) or (15) and (11) is

$$\psi^{(i)} = -\frac{1}{s}\int_\Omega G_i(\mathbf{y},\mathbf{y}')\nabla\cdot\chi(\nabla\psi^{(i)} + \mathbf{e}_i)d\mathbf{y}' = -\frac{1}{s}\int_\Omega G_i(\mathbf{y},\mathbf{y}')\nabla\cdot\chi\nabla(\psi^{(i)} + y_i')d\mathbf{y}' = -\frac{1}{s}\int_\Omega G_i(\mathbf{y},\mathbf{y}')\nabla\cdot\chi\nabla u^{(i)}d\mathbf{y}'. \tag{19}$$

Using Green's first identity and introducing ∇' to denote the gradient with respect to $\mathbf{y}'$, $\nabla' = \nabla_{\mathbf{y}'}$, we write $\psi^{(i)}$ of (19) as

$$\psi^{(i)} = -\frac{1}{s}\int_{\partial\Omega}\chi G_i(\mathbf{y},\mathbf{y}')\nabla' u^{(i)}\cdot\mathbf{n}ds + \frac{1}{s}\int_\Omega \chi\nabla' G_i(\mathbf{y},\mathbf{y}')\cdot\nabla' u^{(i)}d\mathbf{y}'.$$

Noticing the periodicity of χ and boundary conditions of $G_i(\mathbf{y},\mathbf{y}')$ and $u^{(i)}$ on $\partial\Omega$, we obtain

$$\psi^{(i)} = \frac{1}{s}\int_\Omega \chi \nabla' G_i(\mathbf{y},\mathbf{y}') \cdot \nabla' u^{(i)} d\mathbf{y}' = \frac{1}{s}\hat{\Gamma}^i_\chi u^{(i)},$$

where the linear integral operator $\hat{\Gamma}^i_\chi$ is defined as

$$\hat{\Gamma}^i_\chi u^{(i)} = \int_\Omega \chi \nabla' G_i(\mathbf{y},\mathbf{y}') \cdot \nabla' u^{(i)} d\mathbf{y}'. \tag{20}$$

From the definition of the operator $\hat{\Gamma}^i_\chi$, the solution $u^{(i)}$ of the boundary value problem (8) and (9) is given by

$$u^{(i)} = y_i + \psi^{(i)} = y_i + \frac{1}{s}\hat{\Gamma}^i_\chi u^{(i)} \quad (i = 1,2,3). \tag{21}$$

The solution of electric potential $u^{(i)}$ corresponding to the boundary value problem (8) and (9) can be obtained in terms of $\hat{\Gamma}^i_\chi$ and y_i using Eq. (21) so that

$$u^{(i)} = s\left(s\mathbf{I}_3 - \hat{\Gamma}^i_\chi\right)^{-1} y_i \quad (i = 1,2,3). \tag{22}$$

3. Spectral representation for the effective permittivity

In this section, we use solution of the local electric potential problem constructed in the previous section to derive the spectral representation for the effective complex permittivity of a two-component medium and to study fundamental properties of this representation.

Remark 1. Generally, the operator $\hat{\Gamma}^i_\chi$ can have continuous spectrum [30]. To derive a representation with continuous spectrum we could use spectral theorem as it was done in [12,24] for composites with random microgeometry. However, since every measure $\mu(z)$ in (1) can be represented as a weak* limit of a sequence of linear combinations of discrete point measures [29,39], we restrict ourselves by considering the case when $\hat{\Gamma}^i_\chi$ has a discrete spectrum. In this case, the set of eigenvalues is a countable set, and the Stieltjes integral representation (1) reduces to the infinite sum.

We first consider a linear homogeneous boundary-value problem for electric potential $\psi^{(i)}(i = 1,2,3)$ in the domain Ω

$$\nabla \cdot \epsilon \nabla \psi^{(i)} = 0 \tag{23}$$

with the homogeneous Dirichlet and periodic boundary conditions given in (11). Using the material parameter s introduced in (13) and the expression (14) for the scalar complex permittivity ϵ, it can be shown that the electric potential $\psi^{(i)}$ $(i = 1,2,3)$ satisfies the following equation

$$s\Delta\psi^{(i)} = \nabla \cdot \chi \nabla \psi^{(i)} \tag{24}$$

with the same homogeneous Dirichlet and periodic boundary conditions (11). The Green's functions $G_i(\mathbf{y},\mathbf{y}')$ for (24) with periodic boundary conditions (11) solve the problem (16). Using Green's first and second identities, similar to the derivation of (18) through (20), we obtain the homogeneous integral equation

$$\hat{\Gamma}^i_\chi \psi^{(i)} = s^{(i)}\psi^{(i)} \quad (i = 1,2,3). \tag{25}$$

This is an eigenvalue problem with eigenvalue $s^{(i)}$ corresponding to the eigenfunction $\psi^{(i)}$ for the linear integral operator $\hat{\Gamma}^i_\chi$. For each i, solution to the problem is given by a set of eigenvalues and eigenfunctions $s^{(i)}_n, \psi^{(i)}_n$.

We define the space of functions $H^{(i)}_1(\Omega)(i = 1,2,3)$ as follows. Let $H^{\chi,(i)}_1(\Omega)$ be

$$H^{\chi,(i)}_1(\Omega) = \left\{ v^{(i)} | v^{(i)}|_{\partial_{(j-)}\Omega} = v^{(i)}|_{\partial_{(j+)}\Omega},\ j \neq i;\ i,j = 1,2,3;\ v^{(i)} \in H^1(\Omega) \right\}, \tag{26}$$

where the Sobolev space $H^1(\Omega)$ is defined by

$$H^1(\Omega) = \left\{ v | v \in L^2(\Omega),\ \frac{\partial v}{\partial y_k} \in L^2(\Omega),\ k = 1,2,3 \right\} \tag{27}$$

and let us introduce scalar inner product between two electric potential functions $\xi, \zeta \in H^{\chi,(i)}_1(\Omega)$

$$\langle \xi, \zeta \rangle_{H^\chi_1} = \int_\Omega \chi \nabla \xi^* \cdot \nabla \zeta d\mathbf{y}. \tag{28}$$

Here the derivatives are taken in the sense of distributions. We consider the quotient space $H^{(i)}_1 = \left\{ H^{\chi,(i)}_1 / S^{(i)}_1 \right\}$ where $S^{(i)}_1 = \{ v | \langle v, v \rangle_{H^\chi_1} = 0, v \in H^{\chi,(i)}_1(\Omega) \}$ with respect to the introduced inner product. With this definition, we can show that the operator $\hat{\Gamma}^i_\chi$ is a self-adjoint, non-negative, bounded linear operator. The properties of $\hat{\Gamma}^i_\chi$ are stated in the following Theorem 1 through Theorem 4. The detailed proofs of Theorems 1–4 are given in Appendices A, B, C, D.

Theorem 1. *The operator $\hat{\Gamma}^i_\chi$ is a linear self-adjoint operator mapping from $H^{(i)}_1$ to $H^{(i)}_1$.*

In order to show that the integral operator $\hat{\Gamma}^i_\chi$ is non-negative and bounded, we consider the eigenvalue problem

$$\hat{\Gamma}^i_\chi \psi^{(i)}_n = s^{(i)}_n \psi^{(i)}_n, \tag{29}$$

where $\psi^{(i)}_n$ is the solution to the boundary value problem (24) with boundary conditions (11). The eigenvalues $s^{(i)}_n$ have the following properties.

Theorem 2. *All the eigenvalues $s^{(i)}_n$ of the eigenvalue problem (29) are real and lie in the unit interval in the complex s-plane, i.e.,*

$$0 \leqslant s^{(i)}_n < 1. \tag{30}$$

Theorem 3. *Eigenfunctions corresponding to different eigenvalues of $\hat{\Gamma}^i_\chi (i = 1,2,3)$ are orthogonal with respect to the inner product (28).*

We further note that since we consider a case of discrete spectrum (see Remark 1), we can assume that the eigenfunctions $\psi^{(i)}_n$ of (29) corresponding to the eigenvalues $s^{(i)}_n$ ($i = 1,2,3$) form a complete set orthogonal with respect to the scalar inner product (28). Cases were considered in [6–8] as well as Section 18.3 in [36], when the conditions for a complete set of eigenfunctions ψ_n with real eigenvalues s_n, were satisfied. The eigenfunctions $\{\psi^{(i)}_n\}^\infty_{n=1} (i = 1,2,3)$ corresponding to the eigenvalues $s^{(i)}_n$ can be chosen to be orthonormal.

Theorem 4. *The linear integral operator $\hat{\Gamma}^i_\chi (i = 1,2,3)$ is non-negative and bounded in $H^{(i)}_1$.*

To derive the analytical representation for the effective property $\boldsymbol{\epsilon}^*$ in the complex s-plane, we consider a tensor function $\mathbf{F}(s)$ defined as

$$\mathbf{F}(s) = \mathbf{I}_3 - \frac{\boldsymbol{\epsilon}^*}{\epsilon_2} = \mathbf{I}_3 - \frac{1}{\epsilon_2 V}\int_\Omega \epsilon \nabla \mathbf{U} d\mathbf{y}.$$

Using (14) and $\int_\Omega [\nabla \mathbf{U}]_{ij} d\mathbf{y} = V\delta_{ij} (i,j = 1,2,3)$, the tensor $\mathbf{F}(s)$ is rewritten as

$$\mathbf{F}(s) = \frac{1}{sV}\int_\Omega \chi \nabla \mathbf{U} d\mathbf{y}. \tag{31}$$

Suppose that the directions of the applied electric fields $\mathbf{E} = \nabla \mathbf{U}$ coincide with the directions of the principal axes of effective permittivity tensor $\boldsymbol{\epsilon}^*$ and the characteristic function $\chi(\mathbf{y})$ of the first material in the composite is axisymmetric with respect to the spatial coordinates

$$\chi(y'_1, y'_2, y'_3) = \chi(-y'_1, y'_2, y'_3) = \chi(y'_1, -y'_2, y'_3) = \chi(y'_1, y'_2, -y'_3), \tag{32}$$

where

$$y'_1 = y_1 - \frac{L}{2}, \quad y'_2 = y_2 - \frac{L}{2}, \quad y'_3 = y_3 - \frac{L}{2}, \quad \mathbf{y} = (y_1, y_2, y_3)^\top \in \Omega. \tag{33}$$

Then the tensor $\mathbf{F}(s)$ has diagonal form

$$\mathbf{F}(s) = \frac{1}{sV}\int_\Omega \chi\left(\frac{\partial u^{(1)}}{\partial y_1}, \frac{\partial u^{(2)}}{\partial y_2}, \frac{\partial u^{(3)}}{\partial y_3}\right)\mathbf{I}_3 d\mathbf{y}. \tag{34}$$

Let f be the volume fraction of subdomains occupied by the first material and V be the total volume of the composite.

Theorem 5. *Assume that $\psi^{(i)}_n (n = 1,2,\ldots)$ form a complete set of orthonormal eigenfunctions with eigenvalues $s^{(i)}_n$ of the operator $\hat{\Gamma}^i_\chi, i = 1,2,3$. The eigenvalues of the tensor $\mathbf{F}(s) = diag(F_{11}, F_{22}, F_{33})$ have the spectral representation*

$$F_{ii}(s) = \sum_n \frac{A^{(i)}_n}{s - s^{(i)}_n}, \tag{35}$$

where $s^{(i)}_n$ is the n-th simple eigenvalue. The residues $A^{(i)}_n$,

$$A^{(i)}_n = \left|\langle y_i, \psi^{(i)}_n \rangle_{H^\chi_1}\right|^2 \Big/ V \tag{36}$$

satisfy the sum rule:

$$\sum_n A^{(i)}_n = f \tag{37}$$

and the following constraints:

$$0 \leqslant A^{(i)}_n < 1, \; 0 < \sum_n A^{(i)}_n < 1. \tag{38}$$

Proof. See Appendix E. □

The result of Theorem 5 is similar to Bergman's result for the spectral function of isotropic two-component composite [3,4,8].

Remark 2. In general, if the directions of applied electric fields $\mathbf{E} = \nabla\mathbf{U}$ do not coincide with the directions of the principal axes of effective permittivity tensor ϵ^*, the effective permittivity ϵ^* is not a diagonal tensor,

$$\epsilon^* = [\epsilon_{ij}]_{3\times 3} = \frac{1}{V}\int_\Omega \epsilon\nabla\mathbf{U}\mathrm{d}\mathbf{y}. \tag{39}$$

In this case, $\mathbf{F}(s)$ is a tensor function of the form

$$\mathbf{F}(s) = \frac{1}{sV}\int_\Omega \chi \begin{pmatrix} \frac{\partial u^{(1)}}{\partial y_1} & \frac{\partial u^{(2)}}{\partial y_1} & \frac{\partial u^{(3)}}{\partial y_1} \\ \frac{\partial u^{(1)}}{\partial y_2} & \frac{\partial u^{(2)}}{\partial y_2} & \frac{\partial u^{(3)}}{\partial y_2} \\ \frac{\partial u^{(1)}}{\partial y_3} & \frac{\partial u^{(2)}}{\partial y_3} & \frac{\partial u^{(3)}}{\partial y_3} \end{pmatrix} \mathrm{d}\mathbf{y}. \tag{40}$$

Remark 3. We present an alternative proof that the eigenvalues $s_n^{(i)}$ of the eigenvalue problem (29) are real and bounded between zero and one. The eigenvalue s_β of the elliptic problem

$$\nabla\cdot(\epsilon\nabla\psi_\beta) = 0 \Longleftrightarrow s_\beta\Delta\psi_\beta = \nabla\cdot(\chi\nabla\psi_\beta) \tag{41}$$

with homogeneous boundary conditions (11) corresponds to the zero eigenvalue $\lambda_\beta = \epsilon_2 l_\beta$, $\epsilon_2 \neq 0$, of the eigenvalue problem

$$\nabla\cdot(\epsilon\nabla u_\beta) = \lambda_\beta u_\beta \Longleftrightarrow s_\beta\Delta u_\beta = \nabla\cdot(\chi\nabla u_\beta) + l_\beta s_\beta u_\beta \tag{42}$$

subject to the homogeneous boundary conditions (11). Multiplying the differential Eq. (42) by the eigenfunction ψ_β and integrating over the domain Ω, we have

$$s_\beta\int_\Omega \psi_\beta\nabla\cdot(\nabla u_\beta)\mathrm{d}\mathbf{y} = \int_\Omega \psi_\beta\nabla\cdot(\chi\nabla u_\beta)\mathrm{d}\mathbf{y} + l_\beta s_\beta\int_\Omega \psi_\beta u_\beta\mathrm{d}\mathbf{y}.$$

Using integration by parts, this gives

$$s_\beta\left(\int_{\partial\Omega}\psi_\beta\frac{\partial u_\beta}{\partial n}\mathrm{d}\mathbf{s} - \int_\Omega\nabla\psi_\beta\cdot\nabla u_\beta\mathrm{d}\mathbf{y}\right) = \int_{\partial\Omega}\chi\psi_\beta\frac{\partial u_\beta}{\partial n}\mathrm{d}\mathbf{s} - \int_\Omega\chi\nabla\psi_\beta\cdot\nabla u_\beta\mathrm{d}\mathbf{y} + l_\beta s_\beta\int_\Omega\psi_\beta u_\beta\mathrm{d}\mathbf{y}. \tag{43}$$

Accounting for the boundary conditions (11), we obtain the expression of l_β in terms of s_β as

$$l_\beta = \frac{\int_\Omega\chi\nabla\psi_\beta\cdot\nabla u_\beta\mathrm{d}\mathbf{y}}{s_\beta\int_\Omega\psi_\beta u_\beta\mathrm{d}\mathbf{y}} - \frac{\int_\Omega\nabla\psi_\beta\cdot\nabla u_\beta\mathrm{d}\mathbf{y}}{\int_\Omega\psi_\beta u_\beta\mathrm{d}\mathbf{y}}. \tag{44}$$

Define the real and imaginary parts of eigenvalues l_β and s_β as:

$$l_\beta^{\mathrm{R}} = \mathrm{Re}(l_\beta),\quad l_\beta^{\mathrm{I}} = \mathrm{Im}(l_\beta),\quad s_\beta^{\mathrm{R}} = \mathrm{Re}(s_\beta),\quad s_\beta^{\mathrm{I}} = \mathrm{Im}(s_\beta).$$

It follows from (44) that

$$l_\beta^{\mathrm{R}} = \frac{s_\beta^{\mathrm{R}}\int_\Omega\chi|\nabla u_\beta|^2\mathrm{d}\mathbf{y}}{|s_\beta|^2\int_\Omega|u_\beta|^2\mathrm{d}\mathbf{y}} - \frac{\int_\Omega|\nabla u_\beta|^2\mathrm{d}\mathbf{y}}{\int_\Omega|u_\beta|^2\mathrm{d}\mathbf{y}},\quad l_\beta^{\mathrm{I}} = -\frac{s_\beta^{\mathrm{I}}\int_\Omega\chi|\nabla u_\beta|^2\mathrm{d}\mathbf{y}}{|s_\beta|^2\int_\Omega|u_\beta|^2\mathrm{d}\mathbf{y}}. \tag{45}$$

Therefore, the zero eigenvalue (i.e., $l_\beta^{\mathrm{R}} = l_\beta^{\mathrm{I}} = 0$) of the problem (42) implies

$$s_\beta^{\mathrm{I}} = \mathrm{Im}(s_\beta) = 0,\quad 0 \leqslant s_\beta^{\mathrm{R}} = \mathrm{Re}(s_\beta) = \frac{\int_\Omega\chi|\nabla u_\beta|^2\mathrm{d}\mathbf{y}}{\int_\Omega|\nabla u_\beta|^2\mathrm{d}\mathbf{y}} < 1. \tag{46}$$

4. Rational approximation and inversion method

In this section, we propose a new inversion algorithm for reconstruction of the spectral function from known measured data. We solve the inverse problem by constructing a constrained partial fraction decomposition of rational (Padé) approximation calculated using measured values of the effective complex permittivity. The constraints for the poles and residues of the partial fractions are given in (30) and (38). The least squares approximation of the function $\mathbf{F}(s)$ by a rational function was used to construct the Padé approximation.

To derive the numerical scheme of the approximation of the spectral function, we focus on one diagonal component $F(s) = \mathbf{F}_{ii}(s)$ of the tensor $\mathbf{F}(s)$ for simplicity. We note that the function $F(s)$ has a discrete representation in the partial fraction form

$$F(s) = \sum_n \frac{A_n}{s - s_n} \tag{47}$$

as described in previous section after eliminating the superscript i in (35). Here s_n is the n-th simple pole on the unit interval with positive residue A_n. The right hand side of (47) can be approximated by an appropriate rational function

$$\sum_n \frac{A_n}{s - s_n} \simeq \frac{\alpha(s)}{\beta(s)}, \tag{48}$$

where the degree of the polynomial $\alpha(s)$ is lower than the degree of the polynomial $\beta(s)$. We consider the Padé approximation of $F(s)$ (see [2,10])

$$F(s) \simeq F_{[p,q]}(s) = \frac{\alpha(s)}{\beta(s)} = \frac{a_0 + a_1 s + a_2 s^2 + \cdots + a_p s^p}{b_0 + b_1 s + b_2 s^2 + \cdots + b_q s^q}, \tag{49}$$

where a_i and b_j are the coefficients of two real polynomials $\alpha(s)$ and $\beta(s)$ of orders p and q, respectively. Let $\alpha(s)$ and $\beta_1(s)$ be real polynomials of degree p and $q-1$ respectively, with $p \leqslant q-1$. It should be noted that if the pole s_1 is not a zero of $\beta_1(s)$, then there exists a real polynomial $\alpha_1(s)$ with degree $p_1 < q-1$ and a number A_1 such that

$$\frac{\alpha(s)}{\beta(s)} = \frac{\alpha(s)}{\beta_1(s)(s - s_1)} = \frac{\alpha_1(s)}{\beta_1(s)} + \frac{A_1}{s - s_1}. \tag{50}$$

Since all poles $s_n (n = 1,2,\ldots,q)$ of denominator $\beta(s)$ in (49) are simple, by the fundamental theorem of algebra, it is clear that the partial fraction decomposition of the rational function $\alpha(s)/\beta(s)$ holds:

$$\frac{\alpha(s)}{\beta(s)} = \frac{\alpha(s)}{b_q(s - s_1)(s - s_2)\cdots(s - s_q)} = \sum_{n=1}^{q} \frac{A_n}{s - s_n} \quad (b_q \neq 0). \tag{51}$$

We assume that the function $F(s)$ has at least one pole, and use a nonstandard normalization of the polynomial coefficient $b_1 = 1$ in the denominator $\beta(s)$. Given measured data pairs (z_k, f_k) $(k = 1,2,\ldots,N)$, with f_k being the measured value of the function $F(s)$ at the sample point z_k, $f_k = F(z_k)$, and with N being the total number of data points, Eq. (49) can be written as

$$\frac{a_0 + a_1 z_k + a_2 z_k^2 + \cdots + a_p z_k^p}{b_0 + z_k + b_2 z_k^2 + \cdots + b_q z_k^q} = f_k, \tag{52}$$

where $a_i (i = 0,\ldots,p)$, $b_j (j = 0,\ldots,q, j \neq 1)$ are required unknown coefficients. Eq. (52) can be rewritten as

$$a_0 + a_1 z_k + \cdots + a_p z_k^p - b_0 f_k - b_2 f_k z_k^2 - \cdots - b_q f_k z_k^q = f_k z_k \quad (k = 1,2,\ldots,N). \tag{53}$$

Therefore, the unknown real coefficients $a_i (i = 0,\ldots,p)$, $b_j (j = 0,\ldots,q, j \neq 1)$ of the ratio $\alpha(s)/\beta(s)$ are determined by solving the following linear system of equations

$$\mathbf{S}\mathbf{c} = \mathbf{d} \tag{54}$$

where

$$\mathbf{S} = \begin{pmatrix} 1 & z_1 & z_1^2 & \cdots & z_1^p & -f_1 & -f_1 z_1^2 & -f_1 z_1^3 & \cdots & -f_1 z_1^q \\ 1 & z_2 & z_2^2 & \cdots & z_2^p & -f_2 & -f_2 z_2^2 & -f_2 z_2^3 & \cdots & -f_2 z_2^q \\ 1 & z_3 & z_3^2 & \cdots & z_3^p & -f_3 & -f_3 z_3^2 & -f_3 z_3^3 & \cdots & -f_3 z_3^q \\ \cdots & \cdots & \cdots & \cdots & \cdots & \cdots & \cdots & \cdots & \cdots & \cdots \\ 1 & z_N & z_N^2 & \cdots & z_N^p & -f_N & -f_N z_N^2 & -f_N z_N^3 & \cdots & -f_N z_N^q \end{pmatrix},$$
$$\mathbf{c} = [a_0, a_1, \ldots, a_p, b_0, b_2, b_3, \ldots, b_q]^\top, \quad \mathbf{d} = [f_1 z_1, f_2 z_2, \ldots, f_N z_N]^\top \tag{55}$$

and the symbol $[\cdot]^\top$ indicates a transposed matrix. It should be noted that in order to uniquely determine the coefficients $a_i (i = 0,\ldots,p)$, b_j $(j = 0,\ldots,q, j \neq 1)$, the total number of the measurements must be greater or equal to the number of coefficients, i.e., $N > p + q + 1$. The reconstruction problem of determining vector of real coefficients $\mathbf{c}$ in (54) is ill-posed and requires regularization to develop a stable numerical algorithm. In this study we use the constrained minimization method with constraints described above.

To derive solution to the problem (54), we use complex matrices $\mathbf{S} = \mathbf{S}_r + i\mathbf{S}_i$ and $\mathbf{d} = \mathbf{d}_r + i\mathbf{d}_i$ where subindices r and i indicate the real and imaginary parts of the matrices. To solve the problem and obtain a vector of the real Padé coefficients $\mathbf{c}$ we formulate the following least squares problem

$$\min_{\mathbf{c}} \left\{ \|\mathbf{S}\mathbf{c} - \mathbf{d}\|^2 \right\} \Longleftrightarrow \min_{\mathbf{c}} \left\{ \|\mathbf{S}_r\mathbf{c} - \mathbf{d}_r\|^2 + \|\mathbf{S}_i\mathbf{c} - \mathbf{d}_i\|^2 \right\}. \tag{56}$$

Here $\|\cdot\|$ denotes the usual Euclidean norm. The solution of the minimization problem is ill-posed. A widely used approach to regularize the problem is to introduce a penalization term and rewrite the minimization problem (56) as follows [42]

$$\min_{\mathbf{c}} \left\{ \|\mathbf{S}_r\mathbf{c} - \mathbf{d}_r\|^2 + \|\mathbf{S}_i\mathbf{c} - \mathbf{d}_i\|^2 + \lambda^2 \|\mathbf{c}\|^2 \right\}. \tag{57}$$

Here λ is a regularization parameter. The choice of the regularization parameter λ has an important role in solving the regularized problem, since in the dual minimization problem, λ is the Lagrange multiplier by the constraint for the norm of the solution. However, the problem (57) is still ill-posed due to the data noise present in the elements of the matrix $\mathbf{S}$ as well as in the right-hand side vector $\mathbf{d}$. This leads to the problem in which both the coefficient matrix and the right-hand side vector are not precisely known. The total least squares method could be used for solution of this kind of linear least squares problems [19,25]. Application of this method will be discussed elsewhere. Here, we use inequalities (30) and (38) for the residues and poles of the function $F(s)$ to impose constraints for the set of minimizers of the problem. The regularized solution $\mathbf{c}$ for the problem (54) is obtained as a solution of the following constrained least squares minimization problem

$$\begin{aligned} &\min_{\mathbf{c}} \quad \left\{\|\mathbf{S}_{\mathrm{r}}\mathbf{c}-\mathbf{d}_{\mathrm{r}}\|^2+\|\mathbf{S}_{\mathrm{i}}\mathbf{c}-\mathbf{d}_{\mathrm{i}}\|^2+\lambda^2\|\mathbf{c}\|^2\right\} \\ &\text{s.t.} \quad 0\leqslant A_n<1,\ 0\leqslant s_n<1,\ 0<\sum_n A_n^{(i)}<1,\ n=1,2,\ldots,q. \end{aligned} \tag{58}$$

Here parameters A_n and s_n are residues and poles of the partial fractions decomposition (51) of the reconstructed Padé approximation of the spectral function. The corresponding Euler equation is

$$\mathbf{c}=\left\{\mathbf{S}_{\mathrm{r}}^{\top}\mathbf{S}_{\mathrm{r}}+\mathbf{S}_{\mathrm{i}}^{\top}\mathbf{S}_{\mathrm{i}}+\lambda\mathbf{I}_{p+q+1}\right\}^{-1}\left\{\mathbf{S}_{\mathrm{r}}^{\top}\mathbf{d}_{\mathrm{r}}+\mathbf{S}_{\mathrm{i}}^{\top}\mathbf{d}_{\mathrm{i}}\right\}, \tag{59}$$

where $\mathbf{I}_{p+q+1}$ denotes the $(p+q+1)\times(p+q+1)$ identity matrix. After reconstruction of the coefficients a_i $(i=0,\ldots,p)$, b_j $(j=0,\ldots,q, j\neq 1)$ of Padé approximation, its decomposition into partial fractions (51), gives an approximation of the spectral function. Then the volume fraction of the first material in the composite can be calculated using formula (37).

5. Spectral representation for analytical models of composites

In this section, we consider isotropic and anisotropic binary composite materials with specific micro-geometries characterized by cylindrical and ellipsoidal inclusions as well as 3D Bruggeman's symmetric effective-medium composites. We derive analytic representation of the spectral function for such composites to use in numerical simulations.

5.1. Isotropic ellipsoidal microgeometries

Let us consider a microgeometry formed by ellipsoidal inclusions of volume fraction f with a dielectric permittivity ϵ_1 immersed in a much larger homogeneous background with a dielectric constant ϵ_2. The effective permittivity for a three-dimensional isotropic two-component mixture with randomly oriented ellipsoidal inclusions with semiaxes a_x,a_y and a_z (see [40]) is

$$\epsilon^*=\epsilon_2+\epsilon_2\left(\frac{f}{3}\sum_{j=x,y,z}\frac{\epsilon_1-\epsilon_2}{\epsilon_2+N_j(\epsilon_1-\epsilon_2)}\right)\left(1-\frac{f}{3}\sum_{j=x,y,z}\frac{N_j(\epsilon_1-\epsilon_2)}{\epsilon_2+N_j(\epsilon_1-\epsilon_2)}\right)^{-1}, \tag{60}$$

where N_x, N_y and N_z are depolarization factors of the three orthogonal directions, respectively, satisfying $N_x+N_y+N_z=1$. The depolarization factor N_x in the x-direction is given as

$$N_x=\frac{a_xa_ya_z}{2}\int_0^{\infty}\frac{\mathrm{d}t}{(t+a_x^2)\sqrt{(t+a_x^2)(t+a_y^2)(t+a_z^2)}}. \tag{61}$$

The other two depolarization factors, N_y and N_z, are obtained by interchanging a_y and a_x, and a_z and a_x in the above integral.

When three depolarization factors are equal: $N_x=N_y=N_z=1/3$, (60) is reduced to the well-known Maxwell Garnett (MG) formula [31]

$$\epsilon_{\mathrm{MG}}^*=\epsilon_2+3f\epsilon_2\frac{\epsilon_1-\epsilon_2}{\epsilon_1+2\epsilon_2-f(\epsilon_1-\epsilon_2)}. \tag{62}$$

The MG formula (62) predicts the effective permittivity of the mixture with inclusions of spherical shape, which is equivalent to the Hashin–Shtrikman coated spheres (CS) model [26]. We consider two models of composites: mixtures with randomly oriented prolate spheroids (PS) and with randomly oriented oblate spheroids (OS). In these cases, the depolarization factors can be evaluated explicitly. For the prolate spheroids $(a_x>a_y=a_z)$, (61) gives

$$N_x=\frac{1-e^2}{2e^3}\left(\ln\frac{1+e}{1-e}-2e\right),\quad N_y=N_z=\frac{1}{2}(1-N_x), \tag{63}$$

where e is the eccentricity, $e=\sqrt{1-a_y^2/a_x^2}$. For oblate spheroids $(a_x=a_y>a_z)$,

$$N_z=\frac{1+e^2}{e^3}(e-\tan^{-1}e),\quad N_x=N_y=\frac{1}{2}(1-N_z), \tag{64}$$

where $e=\sqrt{a_x^2/a_z^2-1}$.

We use these formulas to find expressions for corresponding spectral functions. The function $F(s)$ corresponding to the effective permittivity defined by the MG formula (62) can be written as

$$F_{\mathrm{MG}}(s) = 1 - \frac{\epsilon^*_{\mathrm{MG}}}{\epsilon_2} = \frac{f}{s-(1-f)/3}. \tag{65}$$

In the complex s-plane, this gives a pole at the location $s = (1-f)/3$ for the spectral function corresponding to $F_{\mathrm{MG}}(s)$. The residue is the volume fraction f of the inclusion material.

The functions $F_{\mathrm{PS}}(s)$ and $F_{\mathrm{OS}}(s)$ corresponding to mixtures with prolate–spheroidal (PS) inclusions (63) and with oblate–spheroidal (OS) inclusions (64), have a similar two-term simple partial fractions form

$$F_{\mathrm{PS(OS)}}(s) = 1 - \frac{\epsilon^*_{\mathrm{PS(OS)}}}{\epsilon_2} = \frac{A_1}{s-s_1} + \frac{A_2}{s-s_2}. \tag{66}$$

Here the parameters s_1, s_2 are the following:

$$\begin{aligned} s_1 &= \frac{1}{2}\left(N_x + N_z - \frac{f}{3} + \sqrt{\left(N_x + N_z - \frac{f}{3}\right)^2 - 4(1-f)N_xN_z}\right), \\ s_2 &= \frac{1}{2}\left(N_x + N_z - \frac{f}{3} - \sqrt{\left(N_x + N_z - \frac{f}{3}\right)^2 - 4(1-f)N_xN_z}\right), \end{aligned} \tag{67}$$

$A_1 = A_1^{PS}, A_2 = A_2^{PS}$ for the prolate spheroid model (PS), and $A_1 = A_1^{OS}, A_2 = A_2^{OS}$ for a mixture with oblate spheroidal (OS) inclusions. These parameters are given as

$$\begin{aligned} A_1^{PS} &= f\left(\frac{s_1 - (2N_x + N_z)/3}{s_1 - s_2}\right), \quad A_2^{PS} = f\left(\frac{s_2 - (2N_x + N_z)/3}{s_2 - s_1}\right), \\ A_1^{OS} &= f\left(\frac{s_1 - (N_x + 2N_z)/3}{s_1 - s_2}\right), \quad A_2^{OS} = f\left(\frac{s_2 - (N_x + 2N_z)/3}{s_2 - s_1}\right). \end{aligned} \tag{68}$$

It is easy to check that the sum rule (37) for the residues in (65) and (66) is satisfied.

5.2. Anisotropic composites with coated elliptical cylinders

As an example of an anisotropic material we consider a two-component mixture with elliptical inclusions of a core phase of an isotropic permittivity ϵ_1 surrounded by a coating of second phase with an isotropic permittivity ϵ_2. The ellipsoid has confocal elliptical interior and exterior surfaces, parameterized in ellipsoidal coordinates by $\rho = \rho_c$ and $\rho = \rho_e$. Let $f < 1$ be the volume fraction of core phase inside the ellipse with surface ρ_c and $1-f$ be the volume fraction of the coating phase between ellipse with the surface ρ_c and inside the larger ellipse with surface ρ_e. The effective permittivity tensor $\boldsymbol{\epsilon}^* = \mathrm{diag}(\epsilon_x^*, \epsilon_y^*, \epsilon_z^*)$ for such a binary mixture with coated ellipsoid inclusions is determined by the formula (see [36]):

$$f\epsilon_2(\boldsymbol{\epsilon}^* - \epsilon_2\mathbf{I}_3)^{-1} = \epsilon_2(\epsilon_1 - \epsilon_2)^{-1}\mathbf{I}_3 + (1-f)\mathbf{M}, \tag{69}$$

where

$$\mathbf{M} = (\mathbf{D}_c - f\mathbf{D}_e)/(1-f), \quad \mathbf{D}_c = (d_{c_1}, d_{c_2}, d_{c_3})\mathbf{I}_3, \quad \mathbf{D}_e = (d_{e_1}, d_{e_2}, d_{e_3})\mathbf{I}_3. \tag{70}$$

Here $\mathbf{D}_c$ and $\mathbf{D}_e$ are the depolarization tensors of the core and exterior elliptical surfaces of the confocal coated ellipsoid. The parameter $d_{c_j} = d_j(c_1, c_2, c_3)$ and $d_{e_j} = d_j(e_1, e_2, e_3)$ ($j = 1,2,3$) are the depolarization factors of the three orthogonal directions with c_j and e_j ($j = 1,2,3$) representing the semi-axis lengths of the core and exterior surfaces of the coated ellipsoid. The expression of these depolarization factors are given in (61).

Let l_1, l_2 and l_3 denote the semiaxis lengths of the core and exterior ellipsoid in the direction of $j = x$, y or z, respectively. In some cases the depolarization factors can be evaluated explicitly. In particular, in the limit as l_3 approaches to ∞, with l_1 and l_2 being held fixed, the depolarization factors d_1, d_2 and d_3 reduce to

$$d_1 = l_2/(l_1 + l_2), \quad d_2 = l_1/(l_1 + l_2), \quad d_3 = 0. \tag{71}$$

Substituting (71) into (70), the tensor matrix $\mathbf{M}$ in (70) becomes

$$\mathbf{M} = \frac{1}{c_1e_1 + c_2e_2}(c_1e_1, c_2e_2, 0)\mathbf{I}_3, \tag{72}$$

so that the effective permittivity tensor $\boldsymbol{\epsilon}^* = \mathrm{diag}(\epsilon_x^*, \epsilon_y^*, \epsilon_z^*)$ for a binary mixture with inclusions of confocal coated elliptical cylinder shape has the form of

$$\epsilon_x^* = \epsilon_2 + \epsilon_2 \frac{f(c_1e_1 + c_2e_2)(\epsilon_1 - \epsilon_2)}{(c_1e_1 + c_2e_2)\epsilon_2 + (1-f)c_1e_1(\epsilon_1 - \epsilon_2)},$$
$$\epsilon_y^* = \epsilon_2 + \epsilon_2 \frac{f(c_1e_1 + c_2e_2)(\epsilon_1 - \epsilon_2)}{(c_1e_1 + c_2e_2)\epsilon_2 + (1-f)c_2e_2(\epsilon_1 - \epsilon_2)},$$
$$\epsilon_z^* = \epsilon_2 + f(\epsilon_1 - \epsilon_2). \tag{73}$$

The analytical expression of the corresponding tensor function $\mathbf{F}(s)$ is given as

$$\mathbf{F}(s) = \mathbf{I}_3 - \frac{\boldsymbol{\epsilon}^*}{\epsilon_2} = (F_x, F_y, F_z)\mathbf{I}_3 = \left(\frac{f}{s - s^x}, \frac{f}{s - s^y}, \frac{f}{s - s^z}\right)\mathbf{I}_3, \tag{74}$$

where the poles s^x, s^y, s^z of the x-, y- and z-components of the density of the spectral measure in the complex s-plane are

$$s^x = \frac{(1-f)c_1e_1}{c_1e_1 + c_2e_2}, \quad s^y = \frac{(1-f)c_2e_2}{c_1e_1 + c_2e_2}, \quad s^z = 0 \tag{75}$$

and the residues are given by the volume fraction f of the inclusion phase. Fig. 2 shows the geometric representation of a cross-section of a two-component mixture with inclusions shaped as coated elliptical cylinders (left) and as coated spheres (right).

5.3. 3D Bruggeman effective-medium approximation model

The Bruggeman effective-medium approximation is one of the mixing rules that is widely used in electromagnetics [7,20,23,38,40,41]. It assumes a model of inhomogeneous material composed of two types of approximately spherical grains with permittivity ϵ_1 and ϵ_2. The derivation of the effective permittivity ϵ^* is based on the assumption of self-consistency which allows to take the permittivity of the matrix material in which the grains are embedded, equal to ϵ^*, and use first order approximation for dilute composite to calculate the resulting effective property. This model is also called self-consistent effective medium approximation (EMA) [36,40].

The function $F_{\mathrm{EMA}}(s)$ for the 3D Bruggeman effective permittivity model has the following form as a function of parameter $s = \epsilon_2/(\epsilon_2 - \epsilon_1)$ on the complex plane [28]:

$$F_{\mathrm{EMA}}(s) = \frac{1}{4s}\left\{3s + 3f - 1 - \sqrt{9s^2 - 6(1+f)s + (1-3f)^2}\right\}. \tag{76}$$

Here f is the volume fraction of sub-domains occupied by the first material with permittivity ϵ_1. Let $\mu(x)$ and $m(x)$ represent the spectral measure and spectral density functions, respectively. The spectral function $F_{\mathrm{EMA}}(s)$ in (76) has an analytic Stieltjes integral representation on the complex plane of variable s, $s = x + iy$, for low volume fraction $f \leqslant 1/3$ the representation has the following form:

$$F_{\mathrm{EMA}}(s) = 1 - \frac{\epsilon^*}{\epsilon_2} = \int_0^1 \frac{\mathrm{d}\mu(x)}{s - x} = \int_0^1 \frac{m(x)\mathrm{d}x}{s - x}. \tag{77}$$

The spectral representation for the three-dimensional Bruggeman self-consistent effective medium analytic model has a continuous spectral density function $m(x)$. The function $m(x)$ is a real non-negative function which is defined in the unit interval $x \in [0,1]$ by the Stieltjes inversion formula:

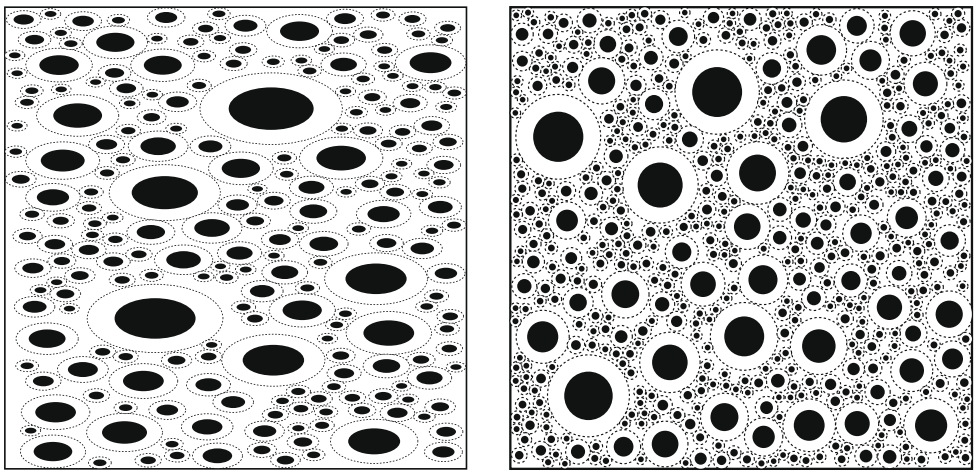

Fig. 2. Cross-sections of a binary mixture with inclusions of coated elliptical cylinders (left) and with coated spheres (right). The illustration shown here is incomplete. The coated elliptical cylinders and coated spheres should fill all space with periodicity on the boundary of domain.

$$m(x) = \frac{\mathrm{d}}{\mathrm{d}x}\mu(x) = -\frac{1}{\pi}\lim_{y\to 0^+}\operatorname{Im} F_{\mathrm{EMA}}(x+\mathrm{i}y). \tag{78}$$

The representation (77) was used to evaluate optical properties of cermets (ceramic–metal mixtures) for $f \leqslant 1/3$ in [28], where the spectral density function $m(x)$ was given as

$$m(x) = \begin{cases} \frac{1}{4\pi x}\sqrt{-9x^2 + 6(1+f)x - (1-3f)^2} & \text{for } x_1 < x < x_2, \\ 0 & \text{otherwise}, \end{cases} \tag{79}$$

where

$$x_{1,2} = \frac{1}{3}\left[1 + f \mp 2\sqrt{2f(1-f)}\right], \quad 0 \leqslant x_1 < x_2 < 1. \tag{80}$$

The function $m(x)$ satisfies the sum rule:

$$\int_{x_1}^{x_2} m(x)\mathrm{d}x = \int_{x_1}^{x_2} \frac{\mathrm{d}\mu(x)}{\mathrm{d}x} = f. \tag{81}$$

The sum rule (81) corresponds to the first moment of the spectral measure $\mu(x)$ and can be used to calculate the unknown parameter of micro-geometry, the volume fraction f, using the reconstructed spectral measure μ as described in Section 4.

6. Numerical examples

This section describes numerical experiments which illustrate the effectiveness of the developed method. We consider isotropic and anisotropic mixtures of silver and silicon dioxide ($AgSiO_2$) and of magnesium and magnesium fluoride ($MgMgF_2$) and simulate frequency dependent measurements using analytic models of composites presented in previous section. We use these simulated measurements as data for the developed Padé approximation method and compare the recovered spectral function with the known analytical model.

The permittivity of silicon dioxide (SiO_2) or magnesium fluoride (MgF_2) considered as the background matrix materials in the mixtures, is taken as a dispersionless constant. The frequency-dependent permittivity of the metallic particles of silver (Ag) or magnesium (Mg) taken as inclusion materials in the composites, is given by the Drude dielectric model (see [27]):

$$\epsilon_1 = \epsilon_{\mathrm{metal}}(\omega) = 1 - \frac{\omega_{\mathrm{p}}^2}{\omega(\omega + \mathrm{i}\gamma)}. \tag{82}$$

Here ω is the circular frequency, ω_{p} is the plasma frequency, γ is the damping constant and $\mathrm{i} = \sqrt{-1}$.

The parameter ω_{p} and the relaxation time $\tau = 1/\gamma$ of the dielectric metallic grains of silver (Ag) and magnesium (Mg) are given in Table 1. The permittivity of background matrix material is $\epsilon_2 = 2.2$ for fused quartz (SiO_2) in the $AgSiO_2$ mixture, and $\epsilon_2 = 1.96$ for magnesium fluoride (MgF_2) in the $MgMgF_2$ mixture. They are shown in Table 1 as well. The frequency-dependent values of the effective complex permittivity ϵ^* for the mixtures of $AgSiO_2$ with silver (Ag) inclusions and of $MgMgF_2$ with magnesium (Mg) inclusions were simulated using described models of microstructure of composite materials.

6.1. Results of computations for isotropic composites

We consider isotropic composites with different microstructure: coated spheres structure given by (62), prolate and oblate spheroids geometry given by (60). The Padé coefficients of the rational function $\alpha(s)/\beta(s)$ were reconstructed using simulated values of the effective complex permittivity ϵ^* at 25 data points in a range of frequency: $0 \leqslant \omega \leqslant \omega_{\mathrm{p}} = 9.4 \times 10^{15}\ \mathrm{s}^{-1}$. These coefficients were used to compute a partial fraction decomposition of $\alpha(s)/\beta(s)$. The partial fraction decomposition gives an approximation to the function $F(s)$ and to the density of the spectral function μ.

Fig. 3 shows results of reconstruction of the density of the spectral function μ. Left Fig. 3 shows results for a composite of 30% of silver (Ag) in silicon dioxide (SiO_2). Right Fig. 3 shows reconstructed spectral densities for a composite of 20% volume of magnesium (Mg) in magnesium fluoride (MgF_2). In both cases, the composites were modeled as isotropic mixtures with coated spherical, prolate–spheroidal and oblate–spheroidal inclusions.

For the isotropic composite with coated spherical inclusions the true delta function solution, which has a pole at the location $s = 0.2333$ with residue $f = 0.3$ for the $AgSiO_2$ mixture and $s = 0.2667$ with residue $f = 0.2$ for the $MgMgF_2$ mixture, is reconstructed almost exactly.

Table 1
Physical parameters of complex permittivity of materials in composites.

Material	γ^{-1}	ω_{p}	Material	Permittivity ϵ_2
Ag	2.5×10^{-15} s	$9.4 \times 10^{15}\ \mathrm{s}^{-1}$	SiO_2	2.20
Mg	2.5×10^{-16} s	$9.4 \times 10^{15}\ \mathrm{s}^{-1}$	MgF_2	1.96

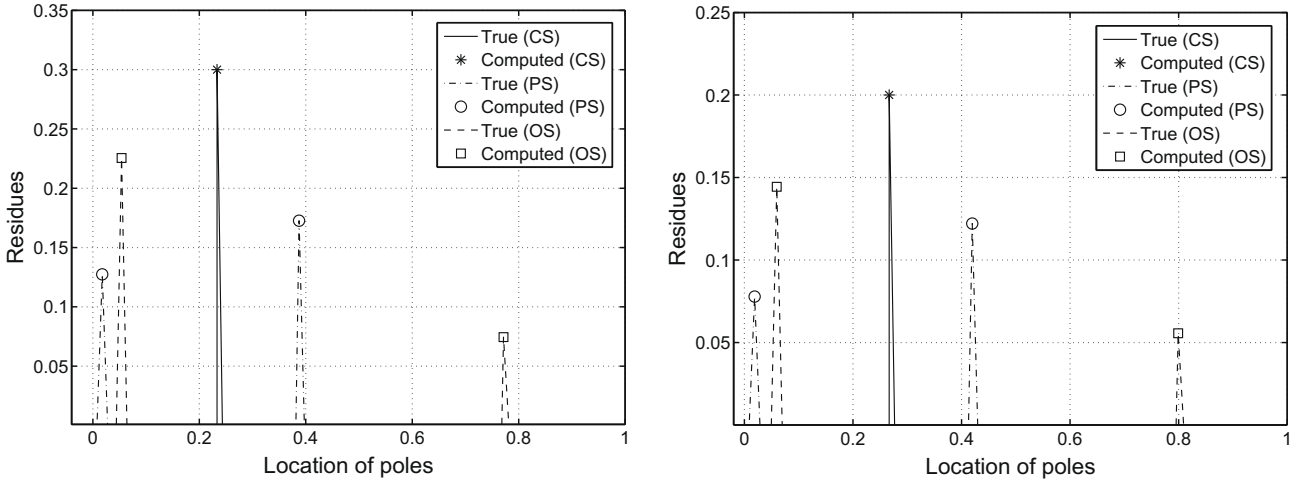

Fig. 3. Reconstruction of residues and poles of the density of the spectral measure μ for composite of 30%Ag–70%SiO_2 (left) and for composite of 20%Mg–80%MgF_2 (right). Coated spherical, prolate spheroidal and oblate spheroidal inclusion structures were used as composite models.

For the models with prolate spheroidal and oblate spheroidal inclusions, the spectral density function has two poles. The true spectral density function found analytically is

$$\mu^*_{ps} = 0.173\delta(s - 0.392) + 0.127\delta(s - 0.018),$$
$$\mu^*_{os} = 0.074\delta(s - 0.776) + 0.226\delta(s - 0.054) \tag{83}$$

for 30%Ag–70%SiO_2 mixture, and

$$\mu^*_{ps} = 0.122\delta(s - 0.425) + 0.078\delta(s - 0.019),$$
$$\mu^*_{os} = 0.056\delta(s - 0.804) + 0.144\delta(s - 0.060) \tag{84}$$

for 20%Mg–80%MgF_2 where $\delta(s)$ is the Dirac delta function. The reconstructed solutions shown in Fig. 3 accurately identify the support of the spectral function as well as its amplitude. The values of the real part and the imaginary part of the complex permittivity ϵ^* for PS-and OS-composites used as data, are shown in Fig. 4 for the 30%Ag–70%SiO_2 mixture and in Fig. 5 for the 20%Mg–80%MgF_2 mixture.

It can be seen from Figs. 4 and 5 that for the $AgSiO_2$ mixture with prolate spheroidal and oblate spheroidal inclusions, the curves of real and imaginary parts of ϵ^* contain two transition points in the ω-plane which correspond to the two poles of spectral density function μ in the complex s-plane. The real and imaginary parts of ϵ^* for the $MgMgF_2$ mixture with prolate spheroidal and oblate spheroidal inclusions show no significant transition points in the ω-plane corresponding to the two poles of the spectral density function μ in the complex s-plane. In spite of this difference, the developed method works equally well in both cases.

6.2. Results for anisotropic composites

Anisotropic composites containing inclusions of coated elliptical cylinders were modeled using formulas (73). Measurements of the effective permittivity were simulated in the same range of frequencies as in previous section. The analytic expression of the true spectral density function μ derived for two anisotropic composite materials are

$$\boldsymbol{\mu}^* = [0.3\delta(s - 0.175), 0.3\delta(s - 0.525), 0.3\delta(s)]\mathbf{I}_3 \tag{85}$$

for 30%Ag–70%SiO_2 mixture, and

$$\boldsymbol{\mu}^* = [0.2\delta(s - 0.2), 0.2\delta(s - 0.6), 0.2\delta(s)]\mathbf{I}_3 \tag{86}$$

for 20%Mg–80%MgF_2 composite material.

The residues and poles of spectral density functions μ_x, μ_y, and μ_z are shown in left Fig. 6 and in left Fig. 7, they are reconstructed very accurately. The computed values of real and imaginary parts of effective permittivity ϵ^*_x and ϵ^*_y are in good agreement with the simulated measurements as shown in right Fig. 6 for the 30%Ag–70%SiO_2 composite and right Fig. 7 for the 20%Mg–80%MgF_2 composite. These results of numerical simulations demonstrate the efficiency of the developed method.

6.3. Results for 3D Bruggeman effective medium

To further verify the effectiveness of the inversion method developed in Section 4, we consider a frequency–dependent metallic particles composite of magnesium (Mg) and magnesium fluoride ($MgMgF_2$) modeled as 3D Bruggeman EMA med-

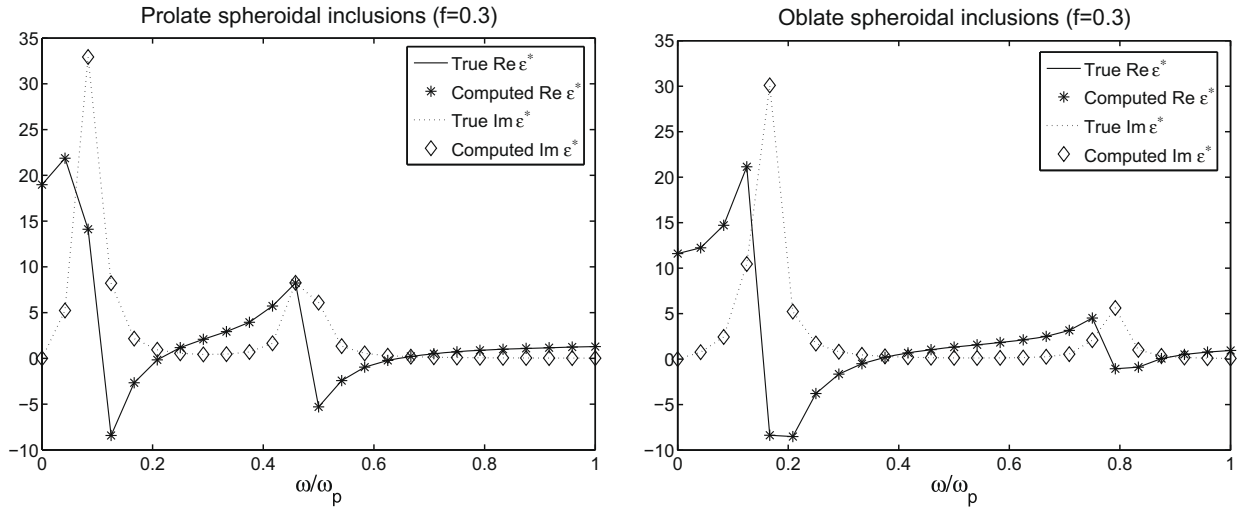

Fig. 4. True and computed real and imaginary parts of effective permittivity ϵ^* as functions of frequency ω/ω_p for mixtures of 30%Ag–70%SiO_2 with two types of inclusions. Left: Isotropic composite with inclusions of prolate spheroid shape. Right: Isotropic composite with inclusions of oblate spheroid shape.

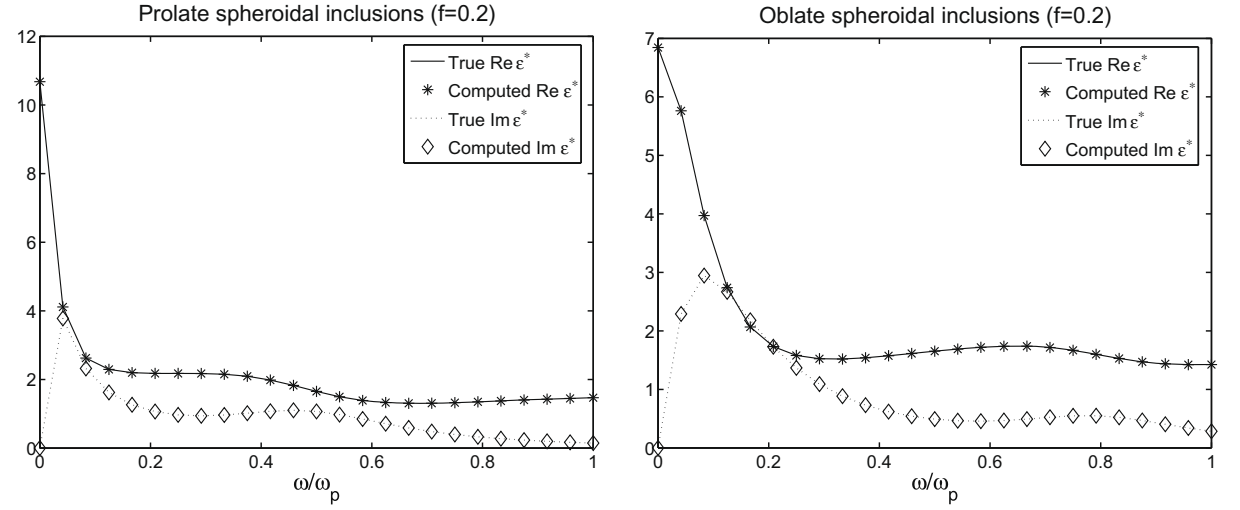

Fig. 5. True and computed real ϵ^* and imaginary ϵ^* for 20%Mg–80%MgF_2 mixture modeled as isotropic composite with inclusions of prolate spheroids shape (left) and oblate spheroids shape (right).

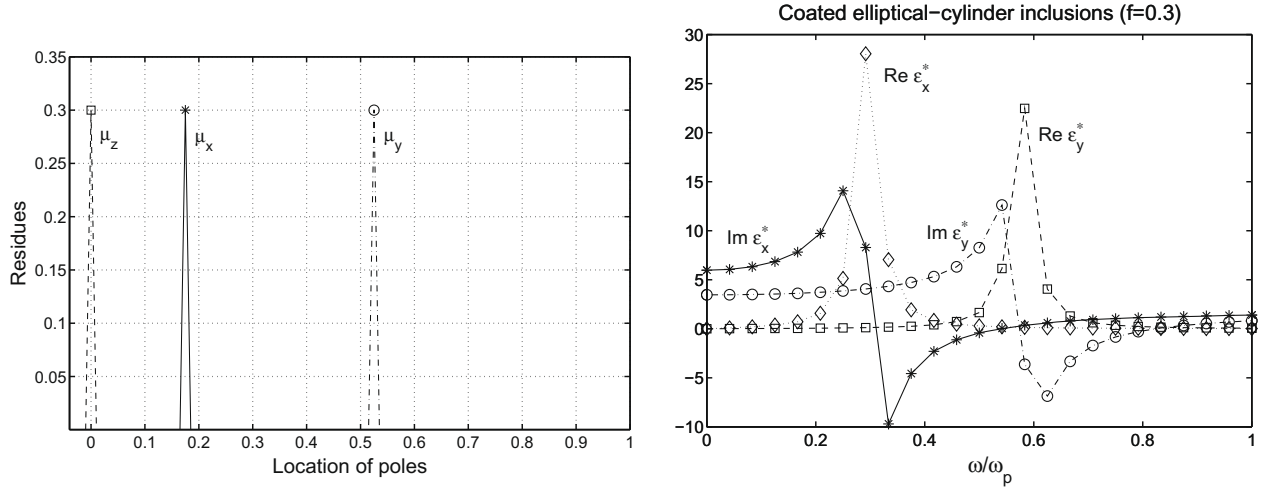

Fig. 6. Results for 30%Ag–70%SiO_2 anisotropic composite with coated elliptical–cylinder inclusions: Left: Reconstructed components μ_x,μ_y, and μ_z of the spectral density function. Right: True and computed real and imaginary parts of ϵ_x^* and ϵ_y^*. (Diamond, square, star, and circle denote the computed values; dotted curve, dashed, solid curve, and dashdot curve represent the true values).

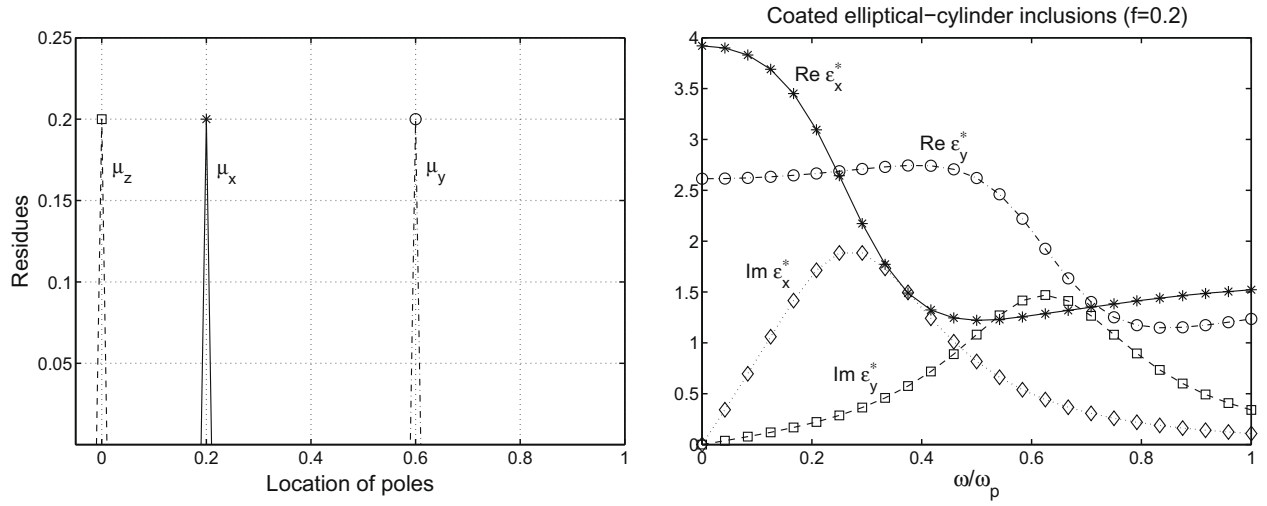

Fig. 7. Results for 20%Mg–80%MgF_2 anisotropic composite with coated elliptical–cylinder inclusions: Left: Reconstructed components μ_x, μ_y, and μ_z of the spectral density function. Right: True and computed real and imaginary parts of ϵ_x^* and ϵ_y^*. (The same symbol agreement as in Fig. 6 is used to represent the computed and true values).

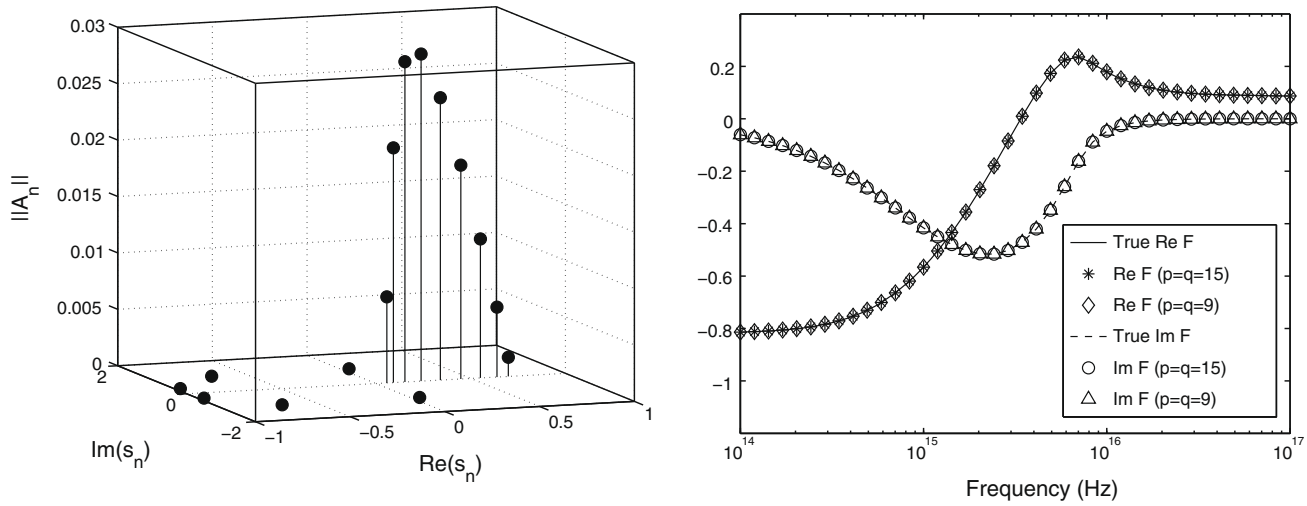

Fig. 8. 3D Bruggeman EMA model of 15%Mg–85%MgF_2 composite. Left: Poles and residues of the spectral measure μ reconstructed without constraints, Padé approximations of order $p = q = 15$. Right: True and computed real and imaginary parts of $F(s)$ ($p = q = 15$ and $p = q = 9$).

ium. The effective permittivity measurements were simulated at 40 data points in the same range of frequencies as in previous examples in Sections 6.1 and 6.2. We considered a composite with volume fraction $f = 0.15$ of Mg component.

The recovered poles and residues of the spectral function for 3D Bruggeman EMA model are shown in the left part of Fig. 8 for the case $p = q = 15$, reconstruction without constraints in the inversion process. The corresponding true and computed real and imaginary parts of $F(s)$ used as data are illustrated in right part of Fig. 8. Left figure in Fig. 9 shows results of reconstruction using constraints in the inversion. It is seen from Figs. 8 and 9 (left) that there are nine valid reconstructed poles which are located between 0.04668 and 0.71998 in the unit interval [0,1), and the other 6 poles are off the unit interval in the complex s-plane.

We also compared analytically and numerically calculated spectral density functions. The right figure of Fig. 9 shows the true spectral density function $m(x)$ and the approximation $\bar{m}(x)$ of the spectral density computed using the Padé approximants of different orders (1) $p = q = 15$ and (2) $p = q = 9$.

The approximation $\bar{m}(x)$ of the spectral density function $m(x)$ at each location of a reconstructed pole s_n with the corresponding residue A_n, is calculated using the following approximation formula

$$\bar{m}(s_n) = \left.\frac{\mathrm{d}\mu(x)}{\mathrm{d}x}\right|_{x=s_n} \approx \frac{A_n}{(s_{n+1} - s_{n-1})/2} \quad (n = 1, 2, \ldots, \bar{q}), \tag{87}$$

where $s_0 = x_1, s_{\bar{q}+1} = x_2$, and $\bar{q}$ is the total number of validly reconstructed poles of the spectral function.

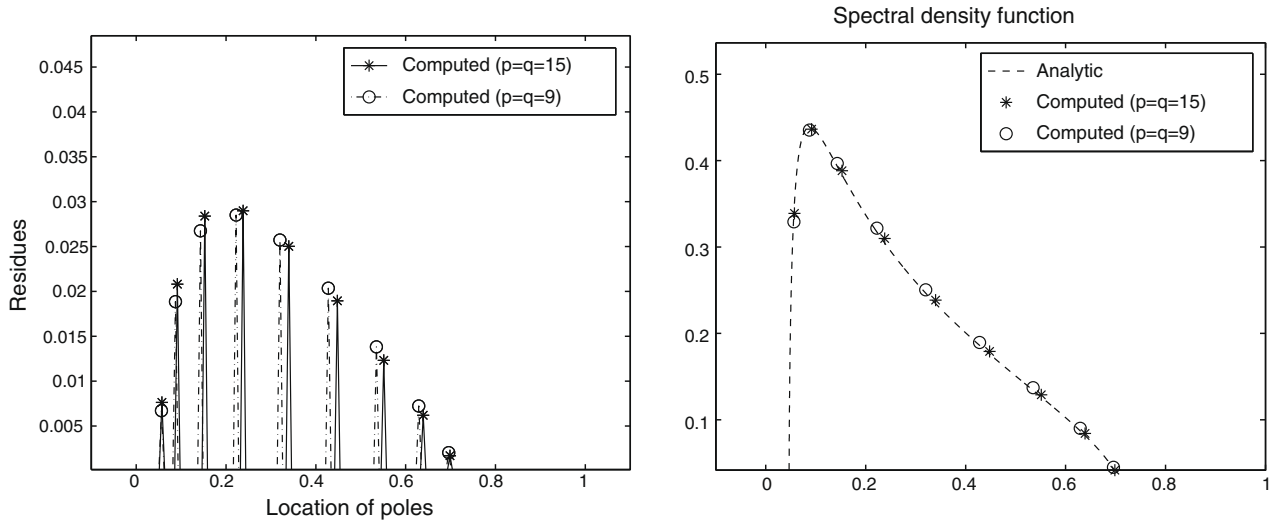

Fig. 9. Reconstructed with constraints poles and residues of the spectral measure $\mu(x)$ (left) and spectral density function $m(x)$ (right) for 3D Bruggeman EMA model of 15%Mg–85%MgF_2 mixture ($p = q = 15$ and $p = q = 9$).

Table 2
Volume fractions calculated for the 3D Bruggeman EMA model using Padé approximation of order $p = q = 7$ and 40 sample data points with added 1%, 3%, 5% noise.

f_{true}	0.05	0.10	0.15	0.20	0.25	0.30
Noise 1%	0.05001	0.09996	0.14955	0.20016	0.25005	0.29922
Noise 3%	0.05031	0.09991	0.14872	0.20075	0.25125	0.30128
Noise 5%	0.05115	0.09984	0.14786	0.20119	0.25211	0.30267

6.4. Stability of reconstruction

The purpose of the next series of computations is to numerically examine the stability of the computational scheme. We calculated the volume fraction of magnesium (Mg) component in the 3D Bruggeman effective medium model of magnesium and magnesium fluoride ($MgMgF_2$) mixture using noisy data. To simulate the errors in the data, we used a uniformly distributed random noise calculated as percentage of the true value of effective permittivity ϵ^* at each of the 40 sample data points at the same range of frequency as described in the beginning of the section. 1%, 3%, and 5% noise was added to the data. A summary of the sensitivity analysis for the calculated volume fraction of the Mg component in $MgMgF_2$ composites of various volume fractions of magnesium phase using noisy data is shown in Table 2. The first row in the table shows the true volume fractions of the magnesium component, while the other three rows present the calculated volume fractions of the magnesium phase. The results of computations show that even with added noise, the recovered volume fractions of magnesium (Mg) component agree with the true values. This demonstrates the stability of the reconstruction algorithm.

7. Conclusion

We developed a numerical inversion method for reconstruction of the spectral measure in Stieltjes representation of the effective complex permittivity of composite material using constrained partial fractions decomposition of Padé approximation. The Stieltjes spectral representation of the effective complex permittivity of a composite factors out the geometric information from dependence of the effective permittivity on the properties of the components. The representation can be reconstructed from the measurements of the effective complex permittivity in a range of frequency of the applied field. We derived a discrete approximation of the spectral function by employing solution to the corresponding boundary-value problem. This gives an extension of the Bergman's spectral representation to three-dimensional anisotropic binary composites. Studying the spectral properties of the operator allowed us to derive the efficient numerical algorithm for constructing a finite dimensional approximation of the spectral measure based on Padé approximation followed by its partial fractions decomposition. The problem is formulated as a constrained least squares minimization problem with regularization constraints provided by the spectral properties of the operator. The method was verified using analytical models of composites with coated cylindrical and ellipsoidal inclusions as well as 3D Bruggeman analytic model which has a continuous spectral density function. The performed numerical experiments for estimation of the fractions of components in a mixture of silver and silicon dioxide and in a composite of magnesium and magnesium fluoride show the effectiveness of the presented

approach. The spectral function recovered from the measurements of effective complex permittivity can be used to evaluate volume fractions of materials in the mixture or other structural parameters of the composite material.

Acknowledgments

The authors are grateful to Graeme Milton for reading the manuscript and providing valuable comments. The authors would also like to thank the reviewers for their comments and constructive suggestions that help to improve the manuscript. This work was supported by NSF Grants DMS-0508901 and DMS-0411035. The first author also acknowledges the support of the sponsors of CREWES and POTSI, funding agencies MITACS, PIMS, and NSERC, and a Postdoctoral Fellowship at the University of Calgary.

Appendix A. Proof of Theorem 1

To show the linearity of the operator $\hat{\Gamma}^i_\chi (i=1,2,3)$, for any two functions $\psi_1^{(i)}, \psi_2^{(i)} \in H_1^{(i)}$ and $\alpha, \beta \in \mathbb{R}$, we have

$$\begin{aligned}\hat{\Gamma}^i_\chi(\alpha\psi_1^{(i)} + \beta\psi_2^{(i)}) &= \int_\Omega \chi\nabla' G_i(\mathbf{y},\mathbf{y}') \cdot \nabla'(\alpha\psi_1^{(i)} + \beta\psi_2^{(i)})\mathrm{d}\mathbf{y}' \\ &= \alpha\int_\Omega \chi\nabla' G_i(\mathbf{y},\mathbf{y}') \cdot \nabla'\psi_1^{(i)}\mathrm{d}\mathbf{y}' + \beta\int_\Omega \chi\nabla' G_i(\mathbf{y},\mathbf{y}') \cdot \nabla'\psi_2^{(i)}\mathrm{d}\mathbf{y}' = \alpha\hat{\Gamma}^i_\chi\psi_1^{(i)} + \beta\hat{\Gamma}^i_\chi\psi_2^{(i)}. \end{aligned} \tag{A.1}$$

In order to show the self-adjoint property of the operator $\hat{\Gamma}^i_\chi$, we notice that the Green's functions G_i are real and satisfy

$$G_i(\mathbf{y},\mathbf{y}') = G_i(\mathbf{y}',\mathbf{y}) \quad (i=1,2,3) \tag{A.2}$$

and for any two functions $\phi^{(i)}, \psi^{(i)} \in H_1^{(i)}$, we have

$$\begin{aligned}\left\langle \hat{\Gamma}^i_\chi\psi^{(i)}, \phi^{(i)} \right\rangle_{H_1^\chi} &= \int_\Omega \chi\nabla\left(\hat{\Gamma}^i_\chi\psi^{(i)}\right)^* \cdot \nabla\phi^{(i)}\mathrm{d}\mathbf{y} = \int_\Omega \chi(\mathbf{y})\left\{\int_\Omega \chi(\mathbf{y}')\nabla\nabla' G_i(\mathbf{y},\mathbf{y}') \cdot \nabla'\left(\psi^{(i)}(\mathbf{y}')\right)^*\mathrm{d}\mathbf{y}'\right\} \cdot \nabla\phi^{(i)}(\mathbf{y})\mathrm{d}\mathbf{y} \\ &= \int_\Omega \chi(\mathbf{y}')\left\{\nabla'\int_\Omega \chi(\mathbf{y})\nabla G_i(\mathbf{y}',\mathbf{y}) \cdot \nabla\phi^{(i)}(\mathbf{y})\mathrm{d}\mathbf{y}\right\} \cdot \nabla'\left(\psi^{(i)}(\mathbf{y}')\right)^*\mathrm{d}\mathbf{y}' = \int_\Omega \chi\nabla'\hat{\Gamma}^i_\chi\phi^{(i)} \cdot \nabla'\left(\psi^{(i)}\right)^*\mathrm{d}\mathbf{y}' \\ &= \left\langle \psi^{(i)}, \hat{\Gamma}^i_\chi\phi^{(i)} \right\rangle_{H_1^\chi}. \end{aligned} \tag{A.3}$$

Therefore, $\langle \hat{\Gamma}^i_\chi\psi^{(i)}, \phi^{(i)}\rangle_{H_1^\chi} = \langle \psi^{(i)}, \hat{\Gamma}^i_\chi\phi^{(i)}\rangle_{H_1^\chi}$ implies that the linear integral operator $\hat{\Gamma}^i_\chi : H_1^{(i)} \to H_1^{(i)}$ is self-adjoint. This completes the proof of theorem. □

Appendix B. Proof of Theorem 2

For each eigenfunction $\psi_n^{(i)}$, rewrite the Eq. (24) as

$$s_n^{(i)}\Delta\psi_n^{(i)} = \nabla\cdot\chi\nabla\psi_n^{(i)} \quad (i=1,2,3; n=1,2,\ldots). \tag{B.1}$$

Multiplying the Eq. (B.1) by $\psi_n^{(i)}$ and integrating over the domain Ω on both sides of this equation, we obtain

$$s_n^{(i)}\int_\Omega \Delta\psi_n^{(i)}\psi_n^{(i)}\mathrm{d}\mathbf{y} = \int_\Omega \nabla\cdot\chi\nabla\psi_n^{(i)}\psi_n^{(i)}\mathrm{d}\mathbf{y}. \tag{B.2}$$

The boundary conditions (11) for the eigenfunction $\psi_n^{(i)}$ and the divergence theorem imply that the inequalities

$$0 \leqslant s_n^{(i)} = \frac{\int_\Omega \chi\nabla\psi_n^{(i)} \cdot \nabla\psi_n^{(i)}\mathrm{d}\mathbf{y}}{\int_\Omega \nabla\psi_n^{(i)} \cdot \nabla\psi_n^{(i)}\mathrm{d}\mathbf{y}} = \frac{\int_{\Omega_1} |\nabla\psi_n^{(i)}|^2\mathrm{d}\mathbf{y}}{\int_\Omega |\nabla\psi_n^{(i)}|^2\mathrm{d}\mathbf{y}} < 1 \tag{B.3}$$

hold. Therefore, all the eigenvalues $s_n^{(i)}$ of the eigenvalue problem (29) are real and are located in the unit interval $s \in [0,1)$. This completes the proof of theorem. □

Appendix C. Proof of Theorem 3

Let $s_n^{(i)}$ and $s_m^{(i)} (m \neq n)$ be eigenvalues of $\hat{\Gamma}^i_\chi (i=1,2,3)$, and let $\psi_n^{(i)}$ and $\psi_m^{(i)}$ be corresponding eigenfunctions. Then

$$\hat{\Gamma}^i_\chi\psi_n^{(i)} = s_n^{(i)}\psi_n^{(i)}, \quad \hat{\Gamma}^i_\chi\psi_m^{(i)} = s_m^{(i)}\psi_m^{(i)}. \tag{C.1}$$

Since $\hat{\Gamma}^i_\chi (i=1,2,3)$ is self–adjoint, and $s_n^{(i)}$ and $s_m^{(i)} (m \neq n)$ are real, we get

$$s_n^{(i)}\left\langle \psi_n^{(i)}, \psi_m^{(i)} \right\rangle_{H_1^\chi} = \left\langle s_n^{(i)}\psi_n^{(i)}, \psi_m^{(i)} \right\rangle_{H_1^\chi} = \left\langle \hat{\Gamma}^i_\chi\psi_n^{(i)}, \psi_m^{(i)} \right\rangle_{H_1^\chi} = \left\langle \psi_n^{(i)}, \hat{\Gamma}^i_\chi\psi_m^{(i)} \right\rangle_{H_1^\chi} = \left\langle \psi_n^{(i)}, s_m^{(i)}\psi_m^{(i)} \right\rangle_{H_1^\chi} = s_m^{(i)}\left\langle \psi_n^{(i)}, \psi_m^{(i)} \right\rangle_{H_1^\chi}. \tag{C.2}$$

Since $s_n^{(i)} \neq s_m^{(i)}$, we must have $\langle \psi_n^{(i)}, \psi_m^{(i)} \rangle_{H_1^\chi} = 0$, which means orthogonality of $\psi_n^{(i)}$ and $\psi_m^{(i)}$. This completes the proof of theorem. □

Appendix D. Proof of Theorem 4

We expand an arbitrary function $\phi^{(i)} \in H_1^{(i)}$ in terms of the orthonormal set of eigenfunctions $\{\psi_n^{(i)}\}_{n=1}^{\infty} (i = 1, 2, 3)$ as

$$\phi^{(i)} = \sum_n \alpha_n \psi_n^{(i)}, \ \alpha_n = \langle \phi^{(i)}, \psi_n^{(i)} \rangle_{H_1^\chi}, \tag{D.1}$$

so that $\langle \phi^{(i)}, \phi^{(i)} \rangle_{H_1^\chi} = \sum \alpha_n^2$. Products $\langle \hat{\Gamma}_\chi^i \phi^{(i)}, \phi^{(i)} \rangle_{H_1^\chi}$ and $\langle \hat{\Gamma}_\chi^i \phi^{(i)}, \hat{\Gamma}_\chi^i \phi^{(i)} \rangle_{H_1^\chi}$ can be represented by sums of products of eigenfunctions, i.e.,

$$\left\langle \hat{\Gamma}_\chi^i \phi^{(i)}, \phi^{(i)} \right\rangle_{H_1^\chi} = \sum_k \alpha_k \left\langle \hat{\Gamma}_\chi^i \psi_k^{(i)}, \sum_n \alpha_n \psi_n^{(i)} \right\rangle_{H_1^\chi} = \sum_k \alpha_k \left\langle s_k^{(i)} \psi_k^{(i)}, \sum_n \alpha_n \psi_n^{(i)} \right\rangle_{H_1^\chi} \tag{D.2}$$

and

$$\left\langle \hat{\Gamma}_\chi^i \phi^{(i)}, \hat{\Gamma}_\chi^i \phi^{(i)} \right\rangle_{H_1^\chi} = \sum_k \alpha_k \left\langle \hat{\Gamma}_\chi^i \psi_k^{(i)}, \sum_n \alpha_n \hat{\Gamma}_\chi^i \psi_n^{(i)} \right\rangle_{H_1^\chi} = \sum_k \alpha_k \left\langle s_k^{(i)} \psi_k^{(i)}, \sum_n \alpha_n s_n^{(i)} \psi_n^{(i)} \right\rangle_{H_1^\chi}. \tag{D.3}$$

Therefore, using Theorem 2 and mutual orthonormality of the eigenfunctions to estimate (D.2) and (D.3), we obtain

$$\left\langle \hat{\Gamma}_\chi^i \phi^{(i)}, \phi^{(i)} \right\rangle_{H_1^\chi} = \sum_k \alpha_k^2 s_k^{(i)} \geqslant 0, \tag{D.4}$$

which shows that $\hat{\Gamma}_\chi^i$ is non-negative, and

$$\left\langle \hat{\Gamma}_\chi^i \phi^{(i)}, \hat{\Gamma}_\chi^i \phi^{(i)} \right\rangle_{H_1^\chi} = \sum_k \alpha_k^2 (s_k^{(i)})^2 \leqslant \sum_k \alpha_k^2 = \left\langle \phi^{(i)}, \phi^{(i)} \right\rangle_{H_1^\chi}, \tag{D.5}$$

which proves that $\hat{\Gamma}_\chi^i$ is bounded. This completes the proof of theorem. □

Appendix E. Proof of Theorem 5

We expand the solution $\psi^{(i)}$ of the boundary-value problem (8) and (9) in series of eigenfunctions $\psi_j^{(i)}$

$$u^{(i)} = \sum_j c_j^{(i)} \psi_j^{(i)}, \tag{E.1}$$

where $c_j^{(i)}$ ($j = 1, 2, \ldots$) are undetermined coefficients. Substituting (29) and (E.1) into (22), we get

$$u^{(i)} = y_i + \frac{1}{s} \hat{\Gamma}_\chi^i \sum_j c_j^{(i)} \psi_j^{(i)} = y_i + \frac{1}{s} \sum_j c_j^{(i)} s_j^{(i)} \psi_j^{(i)} \ (i = 1, 2, 3). \tag{E.2}$$

Taking the inner product with $\psi_n^{(i)} (n = 1, 2, 3, \ldots)$ on both sides of (E.2), we have

$$\left\langle \sum_j c_j^{(i)} \psi_j^{(i)}, \psi_n^{(i)} \right\rangle_{H_1^\chi} = \left\langle y_i, \psi_n^{(i)} \right\rangle_{H_1^\chi} + \frac{1}{s} \sum_j c_j^{(i)} s_j^{(i)} \left\langle \psi_j^{(i)}, \psi_n^{(i)} \right\rangle_{H_1^\chi}. \tag{E.3}$$

Using mutual orthonormality of the eigenfunctions $\psi_j^{(i)}$: $\langle \psi_m^{(i)}, \psi_n^{(i)} \rangle_{H_1^\chi} = \delta_{mn}$ and solving for $c_n^{(i)}$ ($n = 1, 2, \ldots$) in (E.3) for each i, the eigenfunction expansion of $u^{(i)}$ ($i = 1, 2, 3$) is given by

$$u^{(i)} = \sum_n c_n^{(i)} \psi_n^{(i)}, \quad c_n^{(i)} = \frac{s \left\langle y_i, \psi_n^{(i)} \right\rangle_{H_1^\chi}}{s - s_n^{(i)}}. \tag{E.4}$$

Recalling (22) for the expression of $u^{(i)}$ in terms of $\hat{\Gamma}_\chi^i$ and y_i, and noticing (28) and (34), we obtain the component $F_{ii}(s)$ of $\mathbf{F}(s)$

$$F_{ii}(s) = \frac{1}{sV} \int_\Omega \chi \frac{\partial u^{(i)}}{\partial y_i} \mathrm{d}\mathbf{y} = \frac{1}{V} \left\langle (s\mathbf{I}_3 - \hat{\Gamma}_\chi^i)^{-1} y_i, y_i \right\rangle_{H_1^\chi} = \frac{1}{sV} \langle u^{(i)}, y_i \rangle_{H_1^\chi}. \tag{E.5}$$

It follows from (E.4) that

$$F_{ii}(s) = \frac{1}{sV} \sum_n \frac{s \left\langle y_i, \psi_n^{(i)} \right\rangle_{H_1^\chi}}{s - s_n^{(i)}} \left\langle \psi_n^{(i)}, y_i \right\rangle_{H_1^\chi} = \sum_n \frac{A_n^{(i)}}{s - s_n^{(i)}}, \tag{E.6}$$

where $A_n^{(i)} = |\langle y_i, \psi_n^{(i)} \rangle_{H_1^\chi}|^2 / V$, which proves (35) and (36). Expanding the function $y_i (i = 1,2,3)$ in terms of $\psi_n^{(i)}$, i.e.,

$$y_i = \sum_n \beta_n \psi_n^{(i)}, \quad \beta_n = \left\langle y_i, \psi_n^{(i)} \right\rangle_{H_1^\chi},$$

we obtain the scalar inner product

$$\langle y_i, y_i \rangle_{H_1^\chi} = \sum_n \left\langle y_i, \psi_n^{(i)} \right\rangle_{H_1^\chi} \left\langle \psi_n^{(i)}, y_i \right\rangle_{H_1^\chi} = |\left\langle y_i, \psi_n^{(i)} \right\rangle_{H_1^\chi}|^2.$$

Therefore, the sum of all residues $A_n^{(i)}$ is

$$\sum_n A_n^{(i)} = \frac{1}{V} \sum_n \left\langle y_i, \psi_n^{(i)} \right\rangle_{H_1^\chi} \left\langle \psi_n^{(i)}, y_i \right\rangle_{H_1^\chi} = \frac{1}{V} \langle y_i, y_i \rangle_{H_1^\chi}.$$

This last equality together with the scalar inner product $\langle y_i, y_i \rangle_{H_1^\chi} = \int_\Omega \chi \nabla y_i \cdot \nabla y_i d\mathbf{y}$ implies that the sum rule

$$\sum_n A_n^{(i)} = \frac{1}{V} \int_\Omega \chi \mathbf{e}_i \cdot \mathbf{e}_i d\mathbf{y} = f \tag{E.7}$$

holds. Since the volume fraction f of the first component in the mixture is less than one, it is proved that

$$0 \leqslant A_n^{(i)} < 1, \; 0 < \sum_n A_n^{(i)} < 1 \quad (n = 1,2,3\ldots, \; i = 1,2,3).$$

This completes the proof of theorem. □

References

[1] T. Aubin, Nonlinear Analysis on Manifolds, Monge–Ampere Equations, Springer-Verlag, New York, 1982.
[2] G.A. Baker Jr., P. Graves-Morris, Padé Approximations, second ed., Cambridge University Press, 1996.
[3] D.J. Bergman, The dielectric constant of a composite material – a problem in classical physics, Phys. Rep. C 43 (1978) 377–407.
[4] D.J. Bergman, Exactly solvable microscopic geometries and rigorous bounds for the complex dielectric constant of a two-component composite material, Phys. Rev. Lett. 44 (1980) 1285.
[5] D.J. Bergman, Rigorous bounds for the dielectric constant of a two-component composite, Ann. Phys. 138 (1982) 78–114.
[6] D.J. Bergman, Bulk physical properties of composite media, in: Les méthodes de l'homogénéisation: théorie et applications en physique, Eyrolles, Paris, 1985, pp. 1–128.
[7] D.J. Bergman, K.J. Dunn, Bulk effective dielectric constant of a composite with a periodic microgeometry, Phys. Rev. B 45 (1992) 13262–13271.
[8] D.J. Bergman, Hierarchies of Stieltjes functions and their application to the calculation of bounds for the dielectric constant, SIAM J. Appl. Math. 53 (4) (1993) 915–930.
[9] C. Bonifasi-Lista, E. Cherkaev, Analytical relations between effective material properties and microporosity: application to bone mechanics, Int. J. Eng. Sci. 46 (2008) 1239–1252.
[10] E.W. Cheney, Introduction to Approximation Theory, second ed., Chelsea Publishing Company, 1982.
[11] E. Cherkaeva, K.M. Golden, Inverse bounds for microstructural parameters of a composite media derived from complex permittivity measurements, Waves Rand. Media 8 (1998) 437–450.
[12] E. Cherkaev, Inverse homogenization for evaluation of effective properties of a mixture, Inv. Prob. 17 (2001) 1203–1218.
[13] E. Cherkaev, Spectral coupling of effective properties of a random mixture, in: A.B. Movchan (Ed.), IUTAM Symposium on Asymptotics, Singularities and Homogenisation in Problems of Mechanics, Kluwer Academic Press, 2003, pp. 331–340.
[14] E. Cherkaev, D. Zhang, Coupling of the effective properties of a random mixture through the reconstructed spectral representation, ETOPIM Proceedings, Physica B: Physics of Condensed Matter 338 (2003) 16–23.
[15] A.R. Day, M.F. Thorpe, The spectral function of random resistor networks, J. Phys. Condens. Matter 8 (1996) 4389–4409.
[16] A.R. Day, M.F. Thorpe, The spectral function of a composite: the inverse problem, J. Phys. Condens. Matter 11 (1999) 2551–2568.
[17] A.R. Day, M.F. Thorpe, A.R. Grant, A.J. Sievers, The spectral function of a composite from reflectance data, Physica B 279 (2000) 17–20.
[18] C. Engstrom, Inverse bounds and bulk properties of complex-valued two-component composites, SIAM J. Appl. Math. 67 (1) (2006) 194–213.
[19] R.D. Fierro, G.H. Golub, P.C. Hansen, D.P. O'Leary, Regularization by truncated total least squares, SIAM J. Sci. Comput. 18 (4) (1997) 1223–1241.
[20] K.D. Fisher, D. Stroud, Conductivity and magnetoresistance of a periodic composite by network disretization, Phys. Rev. B 56 (4) (1997) 14366–14373.
[21] M. Gajdardziska-Josifovska, R.C. McPhedran, D.J.H. Cockayne, D.R. McKenzie, R.E. Collins, Silver–magnesium fluoride cermet films 1: preparation and microstructure, Appl. Opt. 28 (14) (1989) 2736–2743.
[22] M. Gajdardziska-Josifovska, R.C. McPhedran, D.J.H. Cockayne, D.R. McKenzie, R.E. Collins, Silver–magnesium fluoride cermet films 2: optical electrical properties, Appl. Opt. 28 (14) (1989) 2744–2753.
[23] L. Gao, J.Z. Gu, Effective dielectric constant of a two-component material with shape distribution, J. Phys. D: Appl. Phys. 35 (2002) 267–271.
[24] K. Golden, G. Papanicolaou, Bounds on effective parameters of heterogeneous media by analytic continuation, Commun. Math. Phys. 90 (1983) 473–491.
[25] G.H. Golub, P.C. Hansen, D.P. O'Leary, Tikhonov regularization and total least squares, SIAM J. Matrix Anal. Appl. 21 (1) (1999) 185–194.
[26] Z. Hashin, S. Shtrikman, A variational approach to the theory of the effective magnetic permeability of multiphase materials, J. Appl. Phys. 33 (1962) 3125–3131.
[27] J.D. Jackson, Classical Electrodynamics, Wiley, New York, NY, 1975.
[28] Y. Kantor, D.J. Bergman, The optical properties of cements from the theory of electrostatic resonances, J. Phys. C: Solid State Phys. 15 (1982) 2033–2042.
[29] T. Kato, Perturbation Theory for Linear Operators, Springer-Verlag, 1980.
[30] E. Kreyszig, Introductory Functional Analysis with Applications, John Wiley and Sons, 1989.
[31] J.C. Maxwell-Garnett, Color in metal glasses and in metallic films, Philos. Trans. Roy. Soc. London A203 (1904) 385–420.
[32] R.C. McPhedran, D.R. McKenzie, G.W. Milton, Extraction of structural information from measured transport properties of composites, Appl. Phys. A 29 (1982) 19–27.
[33] R.C. McPhedran, G.W. Milton, Inverse transport problems for composite media, Mater. Res. Soc. Symp. Proc. 195 (1990) 257–274.
[34] G.W. Milton, Bounds on the complex dielectric constant of a composite material, Appl. Phys. Lett. 37 (3) (1980) 300–302.
[35] G.W. Milton, Bounds on the complex permittivity of a two-component composite material, J. Appl. Phys. 52 (8) (1981) 5286–5293.

[36] G.W. Milton, Theory of Composites, Cambridge University Press, 2002.
[37] A.V. Osipov, K.N. Rozanov, N.A. Simonov, S.N. Starostenko, Reconstruction of intrinsic parameters of a composite from the measured frequency dependence of permeability, J. Phys.: Condens. Matter 14 (2002) 9507–9523.
[38] G. Ruossy, E. Spaak, J.M. Thiebaut, Universal equation for the effective complex permittivity of mixtures valid for dielectric–dielectric and dielectric–conductor mixtures, Phys. Rev. B 46 (1992) 11452–11455.
[39] D. Schwartz, Linear Operators, Interscience Publishers, 1963.
[40] A. Sihvola, Electromagnetic mixing formulas and applications, IEE Elect. Waves Ser. Inst. Elect. Eng. London 47 (1999).
[41] D. Stroud, G.W. Milton, B.R. De, Analytical model for the dielectric response of brine-saturated rocks, Phys. Rev. B 34 (1986) 5145–5153.
[42] A.N. Tikhonov, V.Y. Arsenin, Solutions of Ill-posed Problems, Willey, New York, 1977.
[43] A.C. Tripp, E. Cherkaev, J. Hulen, Bounds on the complex conductivity of geophysical mixtures, Geophys. Prosp. 46 (6) (1998) 589–601.
[44] E. Tuncer, Extracting the spectral density function of a binary composite without a priori assumptions, Phys. Rev. B 71 (1) (2005) 012101.
[45] D. Zhang, E. Cherkaev, Padé approximations for identification of air bubble volume from temperature or frequency dependent permittivity of a two-component mixture, Inv. Prob. Sci. Eng. 16 (4) (2008) 425–445.